The Astronomical Journal, 126:1362–1380, 2003 September

THE CENTURY SURVEY GALACTIC HALO PROJECT. I. STELLAR SPECTRAL ANALYSIS

Warren R. Brown[1]
Harvard-Smithsonian Center for Astrophysics, 60 Garden Street, Cambridge, MA 02138; wbrown@cfa.harvard.edu

Carlos Allende Prieto
McDonald Observatory and Department of Astronomy, University of Texas at Austin, Austin, TX 78712

Timothy C. Beers
Department of Physics and Astronomy, Michigan State University, East Lansing, MI 48824

Ronald Wilhelm
Department of Physics, Texas Tech University, Lubbock, TX 79409

and

Margaret J. Geller, Scott J. Kenyon,[1] and Michael J. Kurtz
Smithsonian Astrophysical Observatory, 60 Garden Street, Cambridge, MA 02138
Received 2003 April 14; accepted 2003 May 28

ABSTRACT

The Century Survey Galactic Halo Project is a photometric and spectroscopic survey from which we select relatively blue stars ($V-R < 0.30$ mag) as probes of the Milky Way halo. The survey strip spans the range of Galactic latitude $35^\circ < b < 88^\circ$, allowing us to study the nature of populations of stars and their systematic motions as a function of Galactic latitude. One of our primary goals is to use blue horizontal-branch stars to trace potential star streams in the halo, and to test the hierarchical model for the formation of the Galaxy. In this paper we discuss spectroscopy and multipassband photometry for a sample of 764 blue stars in the Century Survey region. Our sample consists predominantly of A- and F-type stars. We describe our techniques for determination of radial velocities, effective temperatures, metallicities, and surface gravities. Based on these measurements, we derive distance estimates by comparison with a set of calibrated isochrones. We devote special attention to the classification of blue horizontal-branch stars, and compare the results obtained from the application of the techniques of Kinman et al., Wilhelm et al., and Clewley et al. We identify 55 blue horizontal-branch stars. Our large sample of stars also uncovers a number of unusual objects, including three carbon-enhanced stars, a late B-type star located 0.8 kpc above the Galactic plane, and a DZ white dwarf.

Key words: Galaxy: halo — Galaxy: stellar content — stars: abundances — stars: horizontal-branch

On-line material: machine-readable tables

1. INTRODUCTION

The spatial distribution, motion, and composition of halo stars provide a record of the Milky Way's past. A wealth of surveys, including proper-motion– and metallicity-selected surveys of solar-neighborhood stars, surveys of globular clusters and distant giant stars, and pencil-beam surveys of dwarf stars have probed the structure of the halo (e.g., see review by Majewski 1993). These surveys have explored the formation of the halo, the thick disk, and the thin disk, often with dissenting conclusions.

A photometric survey has an advantage over more traditional surveys because there are no selection biases in velocity, proper motion, or metallicity for halo and thick-disk stars. Recent work (Ivezić et al. 2000; Yanny et al. 2000; Vivas et al. 2001; Newberg et al. 2002; Vivas & Zinn 2003) shows that photometric surveys of RR Lyrae and blue horizontal branch stars can reach very deep, and can identify structure in the halo at distances of $\sim$100 kpc. However, these photometric surveys sacrifice both the full six-dimensional kinematic information provided by radial velocities and proper motions and the abundance information that can be obtained from a spectroscopic study. Here we discuss the first results from the Century Survey Galactic Halo Project, a photometric and spectroscopic survey of color-selected stars in the halo and thick disk of the Galaxy.

The Century Survey is a galaxy redshift survey (Geller et al. 1997) for which we obtained 64 deg^2 of V and R imaging to measure a multipassband galaxy luminosity function (Brown et al. 2001). Here we use this CCD photometry to select blue $V-R < 0.30$ mag stars for follow-up spectroscopy. Moderate signal-to-noise (S/N $\approx$ 30) spectra allow us to measure radial velocities, temperatures, surface gravities, and metallicities for the stars, with the goal of probing the nature and the structure of the Milky Way halo and thick-disk populations.

Previous surveys demonstrate that blue horizontal-branch (BHB) stars provide an excellent probe of the halo (Pier 1982; Sommer-Larsen et al. 1989; Preston et al. 1991; Arnold & Gilmore 1992; Kinman et al. 1994; Wilhelm et al. 1999b). One advantage of using BHB stars as tracers is that they are numerous, exceeding the abundance of RR Lyraes by roughly a factor of 10 (Preston et al. 1991). Another advantage is that BHB stars are relatively luminous and hence observable to large distances. Furthermore, BHB

[1] Visiting Astronomer, Kitt Peak National Observatory, National Optical Astronomy Observatory, which is operated by the Association of Universities for Research in Astronomy, Inc., under cooperative agreement with the National Science Foundation.

stars have a small dispersion in absolute magnitude, which makes precise distance estimates possible.

A major difficulty in using BHB stars as probes of Galactic structure is the need to reliably distinguish between low surface gravity BHB stars and the higher surface gravity A-type dwarfs and blue stragglers. BHB stars are core helium-burning stars with lower surface gravities than main-sequence stars of the same spectral type. Although investigators once thought blue stragglers were a minor component of the halo population, recent studies (Norris & Hawkins 1991; Preston et al. 1994; Wilhelm et al. 1999b) demonstrate that a surprisingly large fraction of faint stars in the color range associated with BHB stars are indeed high-gravity stars, many of which are blue stragglers (see Preston & Sneden 2000). Distinguishing BHB stars is particularly important for our blue star sample, which contains a large number of A dwarfs, F dwarfs, and some subgiants. The A and F dwarfs probe the thick and thin disk; the BHB stars probe the inner halo. To distinguish between BHB and A/F dwarfs, we investigate the surface gravity measures of Kinman et al. (1994), Wilhelm et al. (1999a), and Clewley et al. (2002). We compare the results of these three methods, and make our BHB selection based on this comparison.

The $1^\circ \times 64^\circ$ Century Survey photometric strip is located at $8\overset{h}{.}5 < \alpha_{B1950.0} < 13\overset{h}{.}5$, $29^\circ < \delta_{B1950.0} < 30^\circ$. In Galactic coordinates the Century Survey strip cuts across $35^\circ \leq b \leq 85^\circ$, along a line of constant Galactic longitude $l \approx 200^\circ$, before crossing near the north Galactic pole and dropping to $b = 80^\circ$ along $l \approx 50^\circ$ (see Fig. 1). The placement and depth of the Century Survey photometry allows us to address a number of important science goals.

Recent observations and *N*-body simulations lend increasing support to a hierarchical picture where the halo of the Galaxy is composed (at least partially) of tidally disrupted dwarf galaxies (e.g., Searle & Zinn 1978). A good example is the discovery of the Sagittarius dwarf galaxy in the process of tidal disruption by the Milky Way (Ibata et al. 1994). *N*-body models suggest that dwarf galaxies disrupted long ago should still be visible as streams of stars within the Galaxy's halo (Johnston et al. 1996). If the halo potential is spherically symmetric (Ibata et al. 2001), a 90° strip will, in principle, sample one-half of every star stream orbiting the Galaxy, and hence strongly constrain the merger history of the Galactic halo. Thus, the Century Survey Galactic Halo Project is well suited to testing the hierarchical picture for the formation of the Milky Way.

The Century Survey Galactic Halo Project strip spans a wide range of Galactic latitude on both sides of the north Galactic pole and can provide a robust picture of the systematic motions of the thick disk and halo. There is already evidence for systematic motions at all scales in the Milky Way halo. For example, Kinman et al. (1996) found 24 BHB and RR Lyrae stars (out of a sample of 69 stars) streaming toward us from the north Galactic pole with velocity -59 ± 16 km s^{-1}. Majewski et al. (1996) observed large-scale retrograde motion in a deep proper motion sample of 250 halo stars at the north Galactic pole. Gilmore et al. (2002) recently reported evidence for a surprisingly low mean rotational velocity for at least a portion of the thick-disk population, possibly associated with debris from an ancient satellite merger. All of these results are based on surveys which cover only a few square degrees, hence a coherent picture of halo/thick-disk motion is difficult to obtain. As an example of what might be gained from larger area surveys, Yanny et al. (2003) use the Sloan Digital Sky Survey to suggest the presence of a "ring" of stars close to the plane of the Milky Way. This ring might be associated with a tidally disrupted satellite. Interestingly, the bright "metal-weak thick-disk" stars from the study of Beers et al. (2002) exhibit a similar range of metallicity to those inferred for the SDSS ring stars, and kinematics that are similar to the more metal-rich stars of the suggested "intruder population" described by Gilmore et al. (2002).

The placement of the Century Survey photometric region also allows us to establish well-defined, magnitude-limited samples of thin disk/thick disk/halo A-type stars as a function of Galactic latitude (Rodgers 1971; Lance 1988;

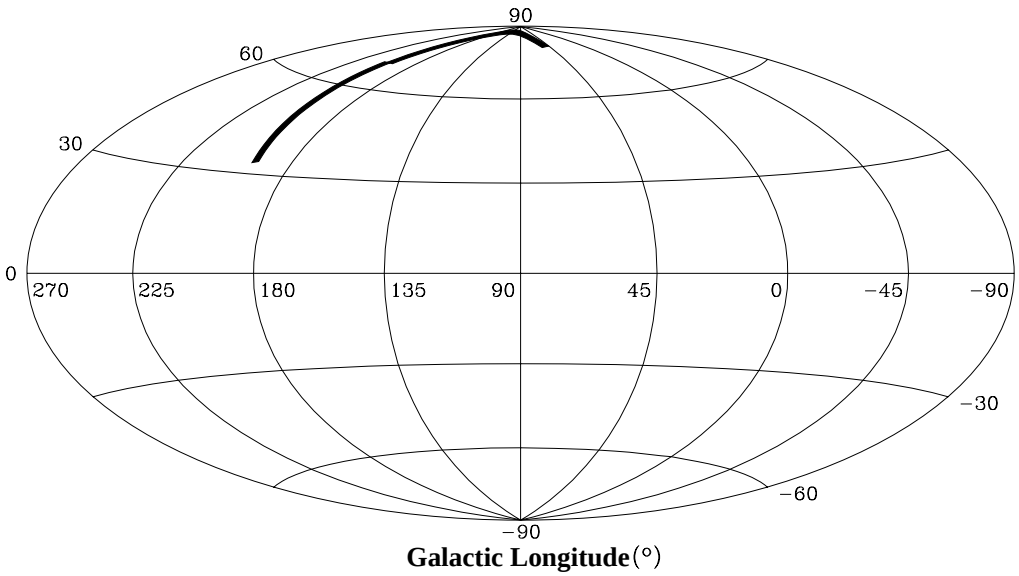

FIG. 1.—Placement of the Century Survey and 2MASS photometric regions in Galactic coordinates. For display purposes we have placed +90° longitude, the direction of the solar orbit around the Galaxy, at the origin.

Rodgers et al. 1993). We will also find distant, high-latitude OB main-sequence stars (Brown et al. 1989; Conlon et al. 1990).

In this paper we discuss the spectroscopic analysis of 764 blue stars from the on-going Century Survey Galactic Halo Project. In § 2 we describe our photometry, spectroscopy, and the efficacy of our sample selection in finding A-type stars. In § 3 we discuss our determinations of radial velocities. In § 4 we describe our methodology for estimation of stellar effective temperatures, surface gravities, and metallicities. In § 5 we describe our stellar classification, and in § 6 we describe our distance estimates. We devote special attention to BHB classification methods in § 7. In § 8 we describe the properties of our sample and list some unusual stellar objects. Our conclusions are presented in § 9.

2. THE SAMPLE

2.1. *Photometry*

The Century Survey photometry is based on Johnson V and Cousins R broadband imaging obtained with the 8 CCD MOSAIC camera (Muller et al. 1998) on the KPNO 0.9 m telescope in 1998 December and 1999 February. The imaging covers a $1\overset{\circ}{.}0 \times 64\overset{\circ}{.}0$ strip located at $8^{\rm h}32^{\rm m}45^{\rm s} < \alpha_{\rm B1950.0} < 13^{\rm h}27^{\rm m}31^{\rm s}$, $29^\circ < \delta_{\rm B1950.0} < 30^\circ$. Brown et al. (2001) includes a detailed description of the data reduction. In brief, the astrometric and photometric solutions are accurate to $\pm 0\overset{''}{.}4$ and ± 0.03 mag, respectively. The average depth of the photometry is $V = 20.3$ mag. The photometric errors are dominated by the zero-point errors at bright magnitudes, resulting in an average color accuracy of $\sigma(V-R) = \pm 0.042$ mag for the $V < 16.5$ mag Century Survey Galactic Halo Project sample selected for spectroscopy.

We obtained *JHK* photometry from the Two Micron All Sky Survey (2MASS) second incremental data release (Skrutskie et al. 2000)[2] for $J < 15$ mag stars in the Century Survey region as well as for stars in a $1^\circ \times 65\overset{\circ}{.}33$ region adjacent to the Century Survey. The adjacent 2MASS region is used to expand the area of the Century Survey Galactic Halo Project. We broke the adjacent region into two pieces to match the available 2MASS photometry: $8\overset{\rm h}{.}5 < \alpha_{\rm B1950.0} < 11\overset{\rm h}{.}25$, $28^\circ < \delta_{\rm B1950.0} < 29^\circ$ and $11\overset{\rm h}{.}25 < \alpha_{\rm B1950.0} < 13\overset{\rm h}{.}5$, $30^\circ < \delta_{\rm B1950.0} < 31^\circ$. Photometry was available for 58.03 deg^2, or 88.8%, of the adjacent 2MASS region. At spectral type A0, the depth of the $J < 15$ mag adjacent 2MASS region is equivalent to $V < 15$ mag. The average $J-H$ error at $J = 15$ mag is $\sigma(J-H) = \pm 0.09$ mag.

Figure 1 shows the placement of the photometric regions in Galactic coordinates. The Century Survey photometry cuts across $35^\circ < b < 85^\circ$ along a line of constant Galactic longitude $l \approx 200^\circ$ (the direction of the Galactic anticenter) before crossing near the north Galactic pole at $b = 88^\circ$ and dropping to $b = 80^\circ$ at $l \approx 50^\circ$. Note that, for display purposes, we have placed $l = 90^\circ$ at the center of Figure 1.

2.2. *Photometric Selection*

Table 1 summarizes the selection of the 764 blue star candidates. We selected the primary sample of stars from the $1^\circ \times 64^\circ$ Century Survey photometry region with $V < 16.5$ mag and $V-R < 0.25$ mag. We also obtained spectra for the redder, brighter [$0.25 \le (V-R) < 0.30$ mag; $V < 15.5$ mag] stars during the spring 2001 observing season. Because the redder stars contained no BHB candidates and outnumbered the $V-R < 0.25$ mag stars by a factor of 2.4, we observed one in 10 of the redder stars in the $V < 16.5$ mag sample during the spring 2002 observing season. The blue $V-R < 0.25$ mag, $V < 16.5$ mag sample selection yields 45% A-type stars and 44% F-type stars.

One hundred eleven of the 764 stars were selected with $J < 15.0$ mag and $J-H < 0.15$ mag from the 2MASS region adjacent to the Century Survey. The 2MASS second incremental data release photometric selection yields 51% A-type stars and 38% F-type stars.

2.3. *Spectroscopy*

We obtained medium-resolution spectra for our sample of 764 blue-star candidates with the FAST spectrograph (Fabricant et al. 1998) on the Whipple Observatory 1.5 m telescope, during the spring 2001 and spring 2002 observing seasons. We use a 600 line mm^{-1} grating and a $2''$ slit to obtain a resolution of 2.3 Å and a spectral coverage from 3400 to 5400 Å. Our exposure times vary; they are designed to reach a signal-to-noise ratio of 30 at 4000 Å. We allow S/N = 15 for objects at $V = 16.5$ mag.

The spectra are processed in the usual way with IRAF.[3] We first subtract a nightly bias frame from the raw images, but only use a dark frame when the dark current exceeds 1 count pixel^{-1} for our exposure times. (The dark current was atypically high for about a month following the UV-illumination of the CCD, a back-side illuminated Loral chip.) We then create a normalization frame by dividing a high-order cubic spline fit from the nightly flat fields. We smooth the bluest 200 Å of the normalization frame with a 3 pixel box to reduce pixel-to-pixel noise in the lower S/N blue end of the flat field.

We extract one-dimensional spectra with the IRAF APEXTRACT package. Wavelength calibrations are determined from helium-argon lamp comparison spectra taken

[2] Available at http://www.ipac.caltech.edu/2mass.

[3] IRAF is distributed by the NOAO, which is operated by AURA, Inc., under cooperative agreement with the NSF.

TABLE 1
OBSERVATIONS

Observed	N	Mag. Limit	Color Selection	Location (B1950.0)
Spring 2001	367	$V < 15.5$	$V-R < 0.30$	$10\overset{\rm h}{.}5 < \alpha < 13\overset{\rm h}{.}5$, $29^\circ < \delta < 30^\circ$
Spring 2002	286	$V < 16.5$	$V-R < 0.25$	$8\overset{\rm h}{.}5 < \alpha < 13\overset{\rm h}{.}5$, $29^\circ < \delta < 30^\circ$
		1 in 10	$0.25 < (V-R) < 0.30$	
Spring 2002	111	$J < 15.0$	$J-H < 0.15$	$8\overset{\rm h}{.}5 < \alpha < 11\overset{\rm h}{.}25$, $28^\circ < \delta < 29^\circ$
				$11\overset{\rm h}{.}25 < \alpha < 13\overset{\rm h}{.}5$, $30^\circ < \delta < 31^\circ$

immediately after each observation. The wavelength solutions use a third-order polynomial fit of ~40 spectral lines, with rms residuals of ±0.07 Å. The spectra are then flux calibrated with nightly standard star observations, usually of Feige 34 or HZ 44 (Massey et al. 1988). The accuracy of the flux calibration is limited by the fact that, for observational efficiency, we do not rotate the slit to the parallactic angle. However, the objects are well placed in the sky at Mount Hopkins: we observe 68% below an air mass of 1.15. The absolute flux calibration is good to 10% for objects observed in photometric conditions; 40% of the objects were observed through light cirrus or in poor seeing and do not have an accurate absolute flux calibration.

3. RADIAL VELOCITIES

We measure stellar radial velocities in two ways, (1) with the cross-correlation package RVSAO (Kurtz & Mink 1998) and (2) by measuring the central wavelengths of several strong lines and comparing them to their rest values. We find an average offset of -0.3 ± 10.4 km s^{-1} between the two methods. The dispersion is consistent with our external error of ±10 km s^{-1}. Our final velocities are an average of the cross-correlation and line-by-line approach.

3.1. *Cross-Correlation*

To implement this approach, we constructed cross-correlation templates from observations of 36 radial-velocity standards. These standards have known velocities accurate to ±0.01 km s^{-1} (Fekel 1999; Stefanik et al. 1999; Udry et al. 1999). We also make use of observations of 25 bright spectral-type standards (Jacoby et al. 1984); the velocities for these stars are from Wilson (1963), and have a typical accuracy of ±2 km s^{-1}.

It is important to have a range of cross-correlation templates because, for a particular observation, a template with a significantly different spectral type produces an asymmetry in the cross-correlation peak and a systematic offset in the measured velocity. We thus bin the observations by spectral subtype to make 16 templates spanning from B through early K. Except for the B templates, there are four or more stars averaged together to construct a template.

The RVSAO package normalizes the 3700–5400 Å region of our spectra for cross-correlation. We find the highest correlation peaks when we multiply the Fourier amplitudes with a cosine-bell filter starting at 20 pixels and running to 1024 pixels. The average internal error from the cross-correlation is ±3.5 km s^{-1}.

We measure our external velocity error by comparing 23 BHB star velocities with velocities published by Kinman et al. (1994). We find a mean +3.5 km s^{-1} offset and a ±19.2 km s^{-1} rms dispersion relative to the Kinman et al. (1994) velocities. Subtracting the published error $\sigma_{\rm Kinman} = \pm 16.2$ km s^{-1} from the measured dispersion of $\sigma_{\rm measured} = \pm 19.2$ km s^{-1} leaves us with an external error of ±10.3 km s^{-1}. This external error is comparable with the dispersion of the individual standard star observations. Standard stars were observed three to five times and had an rms dispersion of ±9.7 km s^{-1}.

We test the effects of decreasing S/N on our cross-correlation measurements by adding Gaussian noise to high-S/N standards. For S/N = 30 at 4000 Å the rms dispersion in velocity is ±6 km s^{-1}; thus, the stars with $V < 15.5$ mag have radial velocity errors dominated by our external error of ±10 km s^{-1}. For S/N = 15 at 4000 Å the rms dispersion in velocity increases to ±15 km s^{-1}; thus, stars at our $V = 16.5$ mag limit have total radial velocity errors approaching ±20 km s^{-1}.

As a further check, we have independently obtained cross-correlation velocities by employing a set of 16 synthetic stellar templates (with, by definition, zero velocity and infinite S/N) covering a range of temperatures, gravities, and metallicities, constructed as described in Wilhelm et al. (1999a). In all cases, the measured cross-correlation velocities obtained by this method are consistent, within the expected errors, with those obtained from the approach above.

3.2. *The "Line-by-Line" Approach*

The line-by-line method optimally locates (using the Gaussian derivative technique described in detail in Beers et al. 1990) the centers of prominent absorption lines in the spectra (e.g., Ca II K, Hδ, Ca I λ4226, Hγ, Hβ), and obtains an averaged radial velocity after pruning of discrepant lines. This method provides a valuable complement to the cross-correlation approach, both as a reality check, and for cases (such as the A-type stars) where the breadth of the Balmer lines results in a "soft" peak in the cross-correlation function. This method also enables extraction of radial velocities for stars that are not well-matched by the range of templates we use in the cross-correlations. Internal errors in this approach are roughly 7–10 km s^{-1}. Extensive tests of the line-by-line method during the course of the HK survey of Beers and colleagues indicate that the external errors are similar.

Appendix Data Table 8 lists the final adopted radial velocities for our program objects. Given our precision, we ignore some of the caveats involved in the definition of radial velocity, but refer the reader to the interesting discussion in Lindegren & Dravins (2003).

4. STELLAR PARAMETERS

The derivation of physical parameters from our observed spectra is basically an optimization problem with a unique solution for effective temperature $T_{\rm eff}$, surface gravity log g, and "metallicity," which we assume to be proportional to the iron abundance, [Fe/H]. We use libraries of synthetic spectra, and search for the set of these parameters that best reproduces a given observation with a genetic algorithm. We compare our results against the independent methods of Beers et al. (1999) and Wilhelm et al. (1999a). We estimate uncertainties in $T_{\rm eff}$, log g, and [Fe/H] by comparing the values from all three methods.

4.1. *Genetic Algorithm*

The spectral range of the Century Survey Galactic Halo Project observations is sufficiently large to provide several indicators of stellar surface temperature. The slope of the observed continuum is mainly dependent on the atmospheric $T_{\rm eff}$. However, the modest accuracy of the flux calibration for the majority of our program stars limits its usefulness. The Balmer-line profiles are also very sensitive to $T_{\rm eff}$, but for earlier spectral types and lower metallicities the lines are significantly affected by gravity and metallicity. In addition, the Balmer lines are difficult to model because their formation depend on (poorly understood) convective energy transport in stellar envelopes.

Fortunately, the wavelength coverage of our spectra extends to include the blue side of the Balmer jump. The Balmer jump not only provides a well-understood gravity indicator, but also serves to decouple the effects of gravity from temperature on the damping wings of the Balmer lines. At a resolving power of $R \sim 2000$, several strong metal lines react mainly to $T_{\rm eff}$ and the metallicity. The Ca II K line is typically saturated at solar metallicity, but it remains as the only reliable metallicity sensitive feature for [Fe/H] $\lesssim -2$. For the warmest and most metal-poor stars in our sample, especially at low S/N, we cannot establish all three parameters with certainty; the sensitivity to metallicity is the first to be lost.

We compare our observed spectra with the low-resolution spectra calculated by Kurucz (1993), based on plane-parallel LTE line-blanketed model atmospheres between 3500 and 5300 Å. We also compute a grid of synthetic spectra with the code SYNSPEC (Hubeny & Lanz 2000)[4] using the same model atmospheres. We compute synthetic spectra with a resolution matching our observations in two windows: 3810–4010 Å and 4700–5000 Å. We use very simple continuum opacities (H, H^-, electron, and Rayleigh scattering). The effect of metals in the continuum is negligible for our combination of spectral range, stellar parameters, and S/N. The 4700–5000 Å window, centered around Hβ, is very effective for stellar classification of F–K stars with solar metallicity and similar-type moderately metal-poor stars (Allende Prieto 2003). The 3810–4010 Å window, which includes the Ca II H and K lines as well as the higher order members of the Balmer series, is useful for extracting physical parameters for the metal-poor A–F stars in our survey.

To reproduce the collisionally enhanced wings of the Ca II lines we adopted damping parameters from Barklem et al. (2000). We also modeled the Balmer lines with new calculations of the absorption coefficients as in Barklem et al. (2002). We vary the microturbulence ξ in the calculation of the $R \simeq 2000$ spectra; its value is fixed at 2 km s^{-1} in the low-resolution spectra computed by Kurucz. The synthetic spectra cover the following range in the stellar parameters:

$$4500 \leq T_{\rm eff} \leq 10,000 \text{ K} , \quad (1)$$

$$2.0 \leq \log g \leq 5.0 \text{ dex} , \quad (2)$$

$$-4.5 \leq [\text{Fe/H}] \leq +0.5 \text{ dex} , \quad (3)$$

$$0 \leq \xi \leq 2 \text{ km s}^{-1} . \quad (4)$$

We assume that the [Mg/Fe] and [Ca/Fe] ratios are solar for [Fe/H] ≥ 0, $+0.4$ for [Fe/H] < -1.5, and vary linearly with declining [Fe/H] between those two ranges.

We use a genetic algorithm (GA; Carroll & Staude 2001) to search over the parameter space and to find the optimal match for each star. The final parameters we adopt are the average of runs using a micro-GA with uniform crossover and a regular GA with creep mutation. We use multilinear interpolation to transform the discrete grid of synthetic spectra into a continuous function for the GA. Figure 2 compares observed and best-matching model spectra for four stars in the sample. Because of the increasing noise, the Balmer lines in the left window have a very low weight in comparison with Hβ. We also assign lower weights to the core of strong (H and Ca II) lines, which are poorly reproduced because of expected departures from LTE in high atmospheric layers. Our metallicity determination for warm and/or metal-poor stars relies on the strength of the Ca II K line and, therefore, we may have large systematic errors for the possible low-metallicity α-poor stars in our sample (Carney et al. 1997; King 1997).

The star CHSS 118 is a good example of a warm metal-poor object. The spectral lines of metallic species in the region around Hβ are almost totally lost in the noise; the strength of the Ca II K line constrains the metallicity. The strength of the Balmer lines is irreconcilable with the continuum slope for this star, probably reflecting a large systematic error in the spectrophotometric calibration. The algorithm gives a higher weight to the Balmer lines than the continuum slope when determining effective temperature. Note that our procedure relies on *relative*, not absolute, fluxes, and we refer to these relative fluxes as *spectrophotometry*. We only rely on the absolute flux calibration of the observed spectra in § 6 to estimate distances.

4.2. *Estimation of* $(B-V)_0$

The $(B-V)_0$ color provides an estimate of effective temperature, and allows us to access independent methods of measuring $T_{\rm eff}$, log g, and [Fe/H]. Although we lack measured B photometry, we can approximate $(B-V)_0$ from the combination of Balmer line strengths and 2MASS $(J-K)_0$ colors, where available. We label this color estimate BV0 to distinguish it from an observed $(B-V)_0$.

First, we employ a neural network approach to estimate BV0 based on observed stellar Balmer-line strengths. We take a large set of stars with available $(B-V)_0$ colors and HP2 and *KP* spectral indices from the HK survey of Beers and collaborators to train the neural network. We include only those stars with inferred reddening $E(B-V) \leq 0.03$ in this training set. Based on comparisons with an extensive validation set of stars (not seen by the neural net during training and testing), we obtain external 0.03–0.035 mag errors in the estimate of BV0, i.e., at the level of the accuracy in the derived reddening corrections.

We use a second neural network to estimate BV0 from 2MASS colors. We train the neural network using a large set of stars from the HK survey with available $(J-K)_0$ and $(B-V)_0$ colors. Here we include only those stars with $E(B-V) \leq 0.03$ and with errors in the J and K magnitudes ≤ 0.04 mag. We train this simple neural network with $(J-K)_0$ as input and $(B-V)_0$ as output, and obtain external errors in the predicted color BV0 of ~ 0.07 mag.

To obtain a final estimated BV0 color, we must first identify stars likely to be bluer or redder than $(B-V)_0 = 0.0$, where the strength of the Balmer lines are greatest, and for which a degeneracy exists blueward and redward of this location when estimating colors from their strengths. We use He I lines to make this separation; these lines are present in the bluer stars and absent in the redder stars. We obtain a final weighted estimate from:

$$\text{BV0} = (3\text{BV0}_{\rm HP2} + \text{BV0}_{\rm 2MASS})/4 ,$$

where $\text{BV0}_{\rm HP2}$ is the prediction based on the Balmer-line strengths and $\text{BV0}_{\rm 2MASS}$ is the prediction based on the 2MASS colors. When 2MASS photometry is not available, we use the $\text{BV0}_{\rm HP2}$ prediction as the final estimate of BV0. Comparison with the observed $(B-V)_0$ colors of the calibrator stars indicates that the final external error in the

[4] Available at http://tlusty.gsfc.nasa.gov.

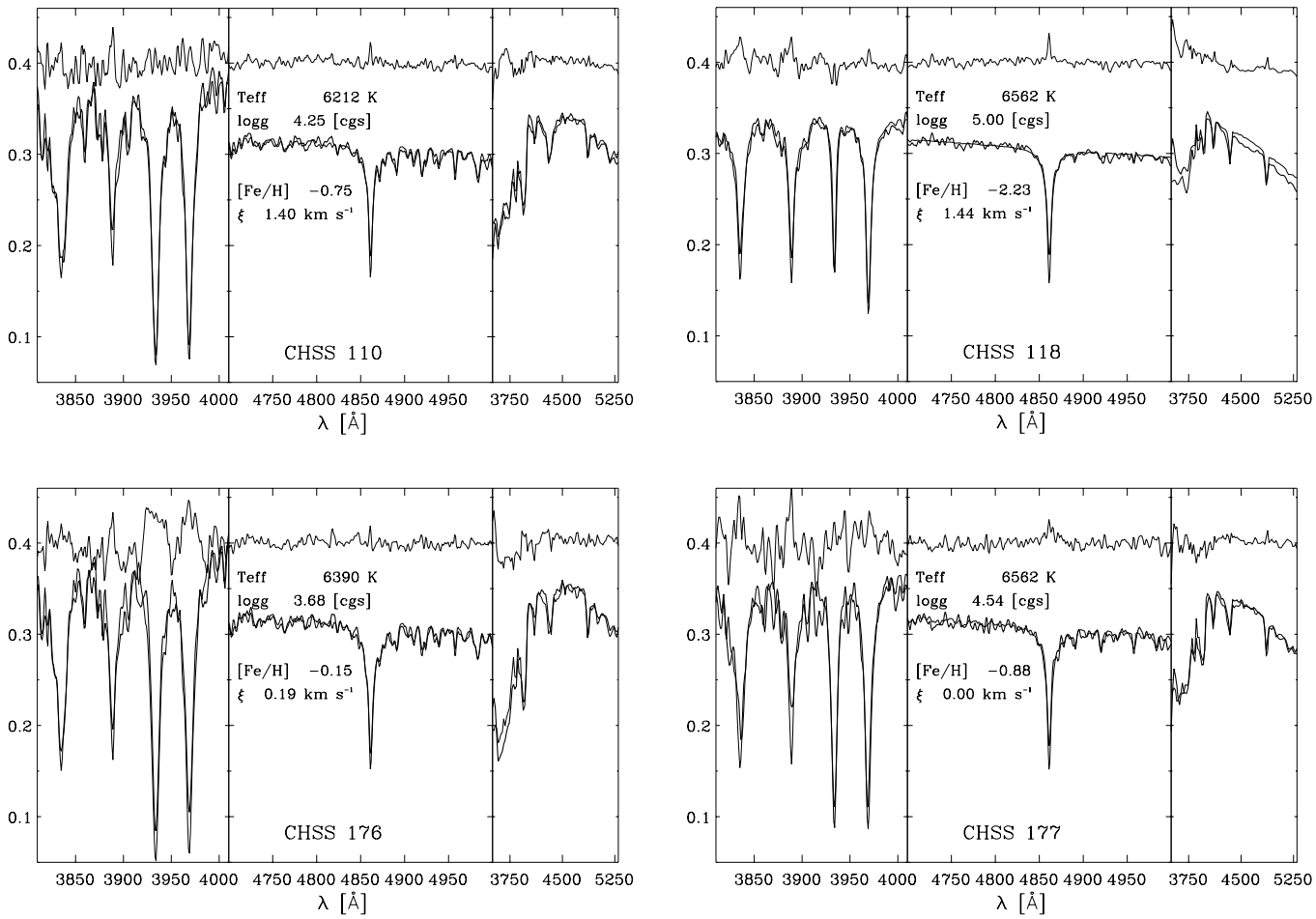

FIG. 2.—Comparison between the observed (*thick line*) and model (*thin line*) spectra for four stars in the sample. We show the observed−model difference (*thinnest line*) shifted by +0.4 above the spectra. The fluxes have arbitrary units. The different windows were independently normalized.

estimated BV0 color is ∼0.04 mag over the color range of the Century Survey stars reported in this paper, and in any case certainly adequate for abundance determination.

4.3. *Comparison of Stellar Parameters and Errors*

Here we compare our values of $T_{\rm eff}$, $\log g$, and [Fe/H] with the those derived from the independent methods of Beers et al. (1999) and Wilhelm et al. (1999a). Although these additional methods rely in part on the same color estimates (as described above), they are complementary to one another since they are calibrated separately, using different sets of comparison stars. Thus, a reasonable estimate of the uncertainties in $T_{\rm eff}$, $\log g$, and [Fe/H] results from a comparison of the values from all three methods.

4.3.1. *Comparison of Stellar Metallicity Estimates*

First, we measure line indices for prominent spectral features (Beers et al. 1999). We then use the line indices to obtain estimates of [Fe/H] and BV0. As a further check, for the stars with sufficiently high S/N spectra, we have made use of the "autocorrelation function" approach (Beers et al. 1999) based on calculations kindly performed for us by John Norris. The autocorrelation function technique is particularly valuable for obtaining stellar metallicity estimates for the cooler, more metal-rich stars in our sample. For such stars, the Ca II KP index can suffer from saturation effects. From the infrared-flux method calibrations of Alonso et al. (1996, 1999) we then derive $T_{\rm eff}$ based on these input estimates.

Second, we follow Wilhelm et al. (1999a) and determine $T_{\rm eff}$ for hot ($T_{\rm eff} > 7000$ K) stars using 2MASS *JHK* photometry and our Johnson *V* photometry. We determine $\log g$ using a combination of the Hδ Balmer-line width (measured at 20% below the local continuum level) and the slope of the Balmer discontinuity. We compare this combination with a grid of synthetic spectra computed using ATLAS9 models and the spectral synthesis routine SPECTRUM (Gray & Corbally 1994). We compute metallicity for the hot stars by comparing the observations to a synthetic grid of equivalent widths for the Ca II K line. We also performed a χ^2 comparison between metallic-line regions in synthetic and observed spectra (Wilhelm et al. 1999a). This latter approach provides valuable information required to identify (in particular) metallic-line A-type stars with peculiar Ca II K line strengths.

Appendix Data Table 9 summarizes the individual metallicity estimates from all three methods. Column (4) is the GA-derived metallicity, denoted as $[{\rm Fe/H}]_{\rm GA}$. Column (5) is the Beers et al. (1999) derived metallicity based on the KP index, $[{\rm Fe/H}]_{\rm KP}$. Column (6) is the Wilhelm et al. (1999a) derived metallicity, $[{\rm Fe/H}]_{\rm EC}$. The designation "EC" arises from the use of both equivalent widths of spectral features and χ^2 spectral matches in deriving the metallicity by this

method. Column (7) lists our best estimate of stellar metallicity, $[Fe/H]_{final}$.

Figure 3 shows that the metallicities of all three methods are in good agreement. We find $[Fe/H]_{KP}-[Fe/H]_{GA} = 0.03 \pm 0.31$, comparing 550 cool stars with $BV0 > 0.3$ mag (and accepted abundance estimates by both techniques). Similarly, we find $[Fe/H]_{EC} - [Fe/H]_{GA} = -0.09 \pm 0.37$, comparing 117 accepted abundances for hot stars with $BV0 \leq 0.3$ mag. Finally, we find $[Fe/H]_{EC} - [Fe/H]_{KP} = -0.12 \pm 0.27$, comparing 536 cool stars with $BV0 > 0.3$ mag. We note that if we ignore the outliers (marked with a colon), the dispersions between the three methods reduce to ± 0.21 dex. Because the final metallicity is an average of two or three of the methods, we believe $[Fe/H]_{final}$ is accurate to ± 0.25 dex.

We employ all three methods to obtain $[Fe/H]_{final}$. For cool stars with $BV0 \geq 0.3$, the KP and GA methods are the primary metallicity indicators. For the hot stars with $BV0 < 0.3$, the GA and EC methods are the primary indicators. In most cases, we obtain $[Fe/H]_{final}$ by a straight average of the appropriate primary indicators, chosen from the three methods (when available). Occasionally (due to either a low S/N spectrum, poor flux calibration, or absent photometry), the primary metallicity estimates are strongly discrepant with one another. We then use the third available method as a tie breaker, and average it with the other indicator with which it best agrees. For a small number of the hot stars where the KP method cannot be used, there remains a large discrepancy between the GA and EC estimates; hence we made choices based on our best guess of which metallicity indicator was led astray (poorly fit spectra, for example, would be one reason to reject the GA estimate). When the final average involves metallicities that disagree by more than 0.4 dex, or when we use only one of the three methods, we indicate some additional uncertainty with a colon next to $[Fe/H]_{final}$. There are a small number of stars where, even after carrying out these procedures, visual inspection of the stellar spectra suggested that the derived final estimate of metallicity was suspect (for example, identification as a metallic-line A star). In such cases we replaced the final metallicity estimate with one that we feel is more likely to be correct than the individual methods suggested (e.g., when we thought it likely that the star was of solar metallicity).

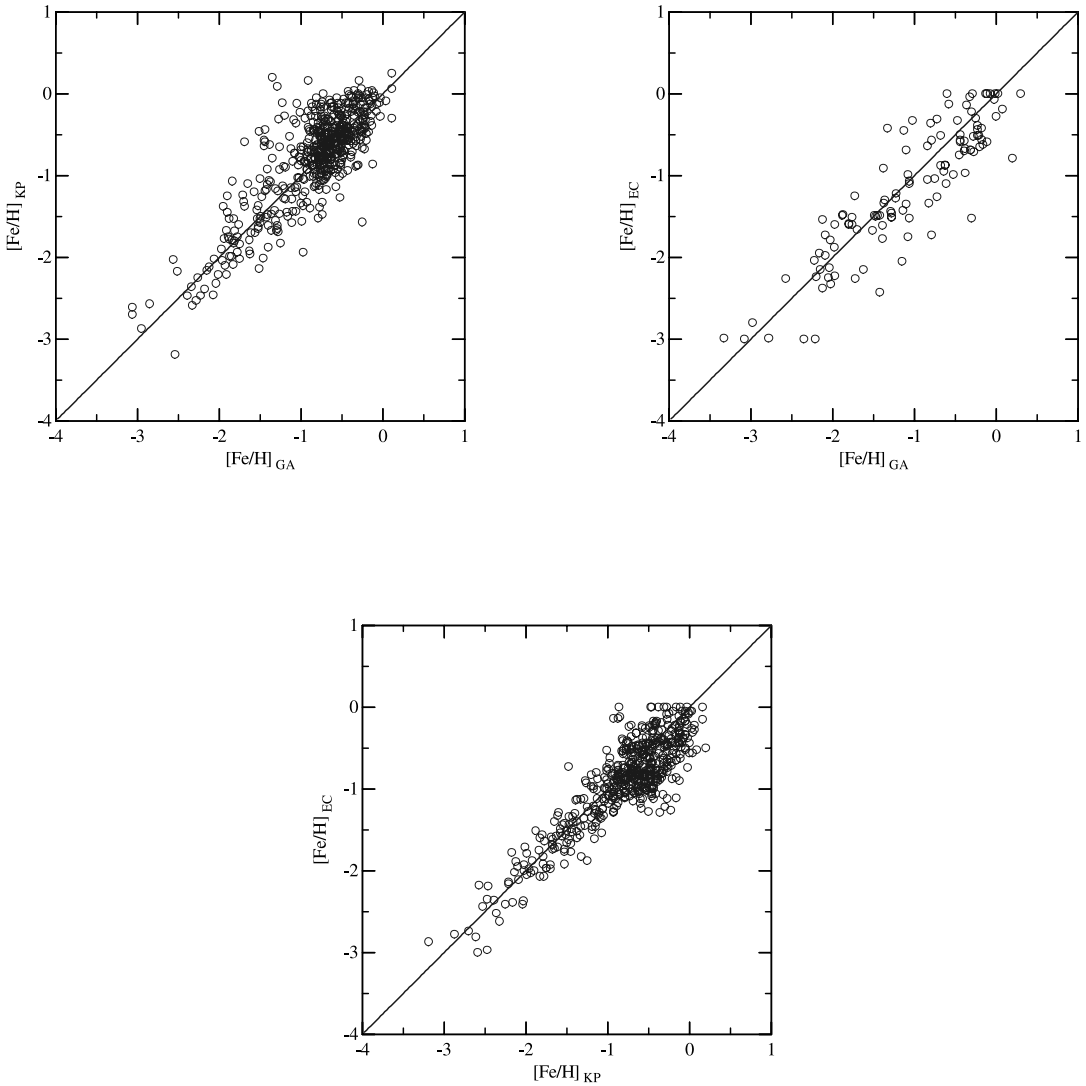

FIG. 3.—Abundance comparison between the three methods used to derive metallicity estimates, which we designate $[Fe/H]_{KP}$, $[Fe/H]_{GA}$, and $[Fe/H]_{EC}$. We conclude that the abundance estimates that we employ are accurate to 0.25 dex (see text).

4.3.2. *Comparison of T_{eff} Estimates*

The temperature estimates obtained from the spectrophotometric and *photometric* $T_{\rm eff}$-values differ significantly: the GA-derived spectrophotometric $T_{\rm eff}$ is higher by 257 K ($\sigma = 196$ K). Because the photometric scale is more robust, we decrease the spectrophotometric $T_{\rm eff}$ by 257 K. We can obtain a third estimate of the effective temperature by combining our V magnitudes with the K magnitudes measured by 2MASS. We use the Alonso et al. (1999) calibrations for this color. We obtain a mean difference $T_{\rm eff}({\rm BV0}) - T_{\rm eff}(V-K) = 116 \pm 9$ K ($\sigma = 212$ K). A bias results from the different zero point between the 2MASS and Johnson K bandpasses. We thus correct the $(V-K)$-based $T_{\rm eff}$-values to the BV0 scale. We note that the Alonso et al. (1999) scales are limited to $5000 \lesssim T_{\rm eff} \lesssim 8000$ K; we cannot check for systematic differences outside this range.

Figure 4 compares the photometric and spectrophotometric temperatures. The solid lines indicate the mean shifts. Whenever the BV0 or $V-K$ calibrations could be used, we considered them in the final $T_{\rm eff}$ estimate.

4.3.3. *Comparison of log g Estimates*

We finally compare the GA-derived gravities with those determined with the Wilhelm et al. (1999a) method described here. The GA gravities are higher by 0.26 dex, with a standard deviation of 0.35 dex. We deem this difference reasonably good, considering the difficulty of estimating surface gravity from medium-resolution spectra. We adopt the GA-derived gravities as our final value of log g and estimate the error to be 0.25 dex.

In summary, our values of $T_{\rm eff}$, log g, and [Fe/H] are uncertain by roughly 200 K, 0.4 dex, and 0.25 dex, respectively. Appendix Data Table 9 lists the adopted values of the physical parameters for our program stars.

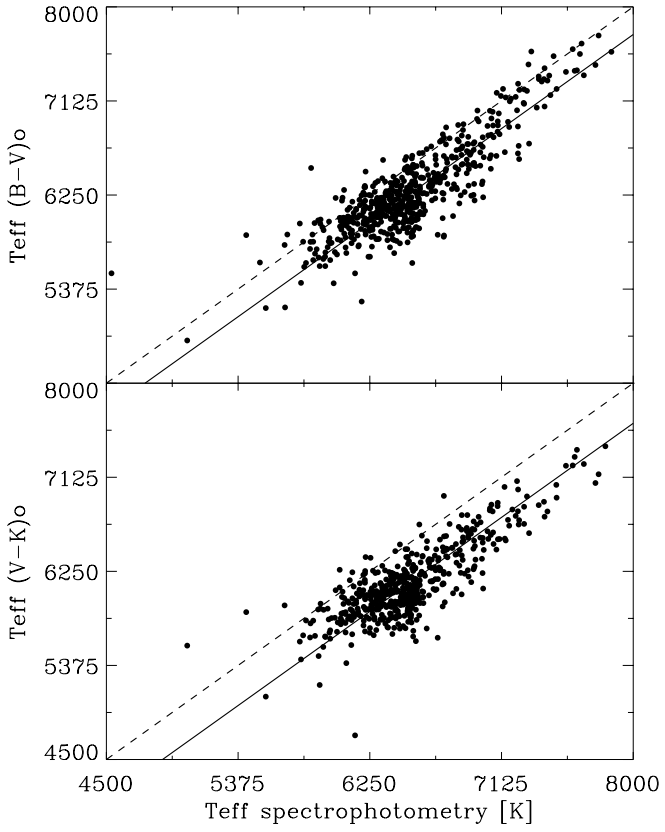

FIG. 4.—Photometric $T_{\rm eff}$'s plotted against the GA-derived spectrophotometric $T_{\rm eff}$. The dashed lines have a slope of one. The solid lines indicate the mean shifts.

5. SPECTRAL CLASSIFICATION

In addition to the stellar parameters described in § 4, stellar spectral classification provides a useful way to organize the stars in our sample. BHB stars, for example, typically have an early A-type spectral classification, while the cooler stars are typically of later classes. We perform spectral classification by measuring the relative strengths of absorption lines in the stellar spectra, and make use of the stellar spectral line indices of O'Connell (1973) and Worthey et al. (1994). We determine spectral types from line-index versus spectral-type relations that we have derived for the Jacoby et al. (1984) library of (luminosity class V) stellar spectra.

Table 2 summarizes the line-index versus spectral-type relations we employ. Our spectral classifications are based primarily on the Ca II λ3933 line index and the $H_{\rm sum}$ line index—a sum of the H λ3889, H λ4101, H λ4340, and H λ4861 line indices. As an example, Figure 5 shows the Ca II line-index bands (O'Connell 1973) overlaid on an A and an F stellar spectrum from our data set. We use the CN λ3860, CH λ4305, Mg I λ5175, and $Fe_{\rm sum}$ line indices to extend our spectral classification range and to corroborate the type obtained from the Ca II and $H_{\rm sum}$ line indices. In practice, each spectral classification typically depends on four spectral line indices, and has an uncertainty of ± 1.1 spectral subtypes.

Because the Jacoby et al. (1984) library largely contains solar-metallicity stars, the line index versus spectral type relations are appropriate for stars of solar metallicity. There are systematic offsets in spectral types for the metal poor stars; as a result the effective temperatures for the most metal-poor stars in our sample are 1000 K too low for the spectral types we measure. Recognizing this difficulty with the spectral types, we use them only to separate A-type stars from F-type stars, and to identify unusual objects.

6. DISTANCE ESTIMATES

We estimate distances to our stars in two ways. For the likely BHB stars in the sample, we employ our broadband photometry and published luminosity-metallicity relations to provide reasonably precise distance estimates. For the rest of the sample, we use estimates of stellar angular diameter and stellar radius from theoretical isochrones to provide rough distance estimates.

6.1. *BHB Distances*

Published M_V-metallicity relations for horizontal-branch stars vary considerably, with values of the slope ranging between 0.15 (Carney et al. 1992) and 0.30 (Sandage 1993). Values of the zero point fall into two groups, $\sim$0.30 mag apart. Fortunately, a search for star streams only requires *relative* distances. Thus, we do not concern ourselves with the exact zero-point of the M_V-metallicity relation.

We use the *Hipparcos*-derived zero point, $M_V({\rm RR}) = 0.77 \pm 0.13$ mag at [Fe/H] $= -1.60$ (Gould & Popowski 1998), based on the statistical parallax of 147 halo RR

TABLE 2
SPECTRAL LINE INDICES

Spectral Line Index[a]	Spectral Type[b]	Valid Range[c]	rms[d]
Ca II λ3933	21.4 + 26.3 Ca II	22 < st < 40	±1.1
H_{sum} =			
H $\lambda\lambda$(3889 + 4101 + 4340 + 4861)	42.2 − 6.98 H_{sum}	22 < st < 39	±1.4
	5.23 + 5.97 H_{sum}	9 < st < 22	±1.4
CN λ3860	37.2 + 24.2 CN	35 < st < 43	±1.5
	7.58 − 79.0 CN	9 < st < 17	±1.5
CH λ4305	28.6 + 43.9 CH	33 < st < 42	±2.0
	16.5 + 93.6 CH	1 < st < 26	±2.0
Mg I λ5175	29.1 + 90.1 Mg I	34 < st < 52	±2.3
Fe_{sum} =			
Fe $\lambda\lambda$(4383 + 4531 + 5015 + 5270)	23.6 + 73.0 Fe_{sum}	25 < st < 48	±2.3

[a] The line indices (e.g., Ca II) are flux ratios normalized by bandwidth of the flux in a stellar spectral line band divided by the flux in nearby continuum side bands. See O'Connell 1973 and Worthey et al. 1994 for the band definitions.
[b] Fits based on luminosity class V stellar spectra from Jacoby et al. 1984.
[c] Spectral types are quantified as B0 = 10, A0 = 20, F0 = 30, etc.
[d] The rms residual of the least-squares fit used as the weight for the spectral classification.

Lyrae field stars. We employ the recently measured M_V-metallicity slope 0.214 ± 0.047 (Clementini et al. 2003), based on photometry and spectroscopy of 108 RR Lyrae stars in the Large Magellanic Cloud. We use the resulting relation, $M_V(\mathrm{RR}) = 0.214[\mathrm{Fe/H}] + 1.11$ mag, to calculate distances to the BHB stars. We note that this empirical relation yields absolute magnitudes 0.21 ± 0.03 mag less luminous than the theoretical ZAHB relations of

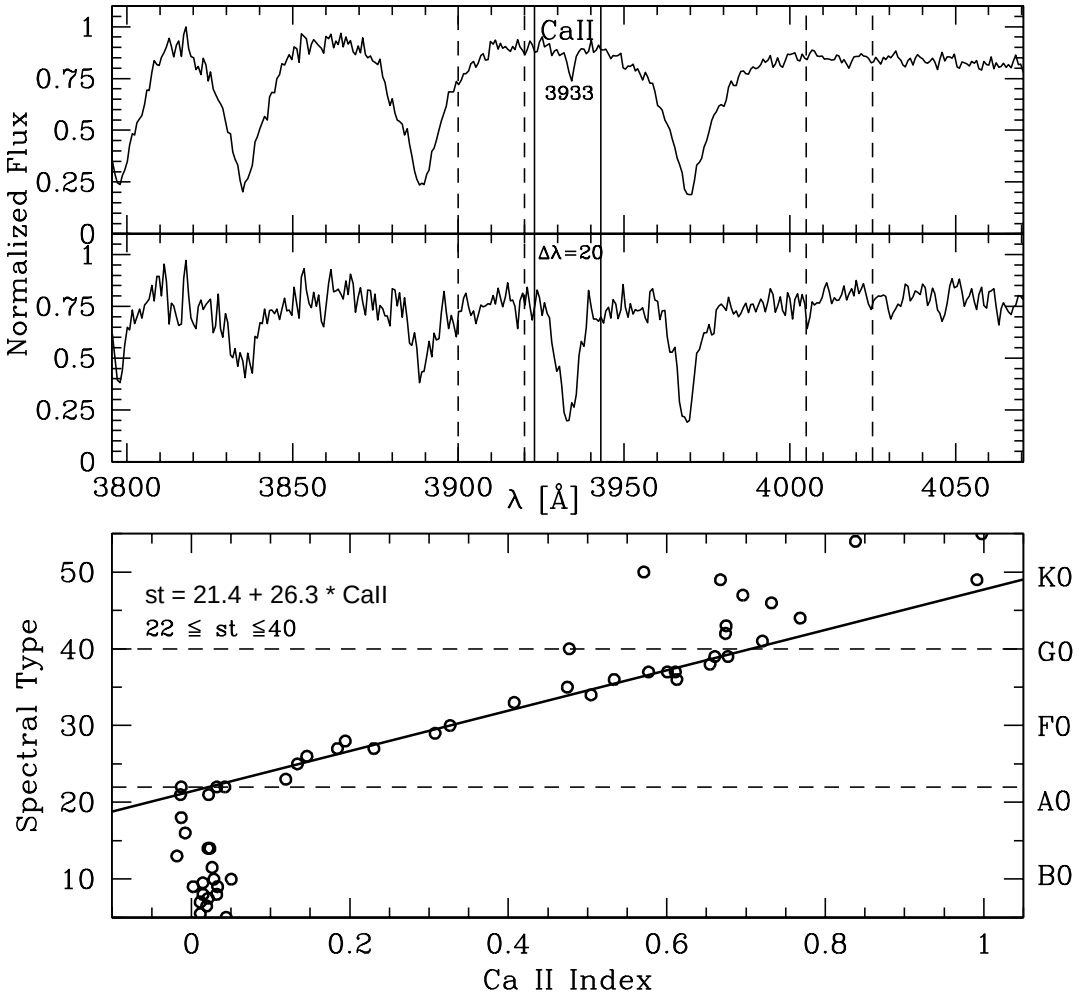

FIG. 5.—*Top*: O'Connell (1973) Ca II λ3933 spectral line-index band and sidebands, plotted on an A and F star spectra. *Bottom*: Line index values measured for the Jacoby et al. (1984) library of luminosity class V stellar spectra. The spectral type relation is valid between A2 and G0, with a residual of ±1.1 spectral subtypes.

Caloi et al. (1997), Salaris et al. (1997), and Cassisi et al. (1999) over the metallicity range $-3 < [Fe/H] < 0$ of our BHB stars. Appendix Data Table 9 lists the distances for the BHB stars.

6.2. *Non-BHB Distances*

We derive rough distances to the non-BHB stars in our sample using estimates of stellar angular diameter, θ, and stellar radius, R. The absolute fluxes and the derived stellar parameters for our stars allow a direct estimate of the stellar angular diameter from

$$\theta \simeq 2\sqrt{\frac{f_\lambda}{F_\lambda(T_{\rm eff}, \log g, [{\rm Fe/H}])}}\,, \qquad (6)$$

where f_λ is the observed flux at Earth and $F_\lambda(T_{\rm eff}, \log g, [Fe/H])$ is the flux at the stellar surface predicted by a model atmosphere. We can obtain a second estimate of the angular diameter θ by following di Benedetto (1998), who derived a Barnes-Evans relation between the surface brightness and the $(V-K)_0$ color for spectral types in the range ~A0 to G2. Before applying this approach, we correct for the systematic offset of 0.07 mag in the $(V-K)_0$ color as explained in § 4.

Stars at a given locus in the HR diagram have a limited range of stellar radius R. By using stars in eclipsing binary systems with radii known to less than 2%, Allende Prieto & Lambert (1999) find that the position in the $(B-V)$-M_V plane can constrain the stellar radius R to ~8% for nearby solar-metallicity stars. Similarly, the position of a star in $T_{\rm eff}$-log g-[Fe/H] space provides a useful means to estimate the stellar radius R, and we exploit our spectroscopic determinations of these parameters to this end. We use the isochrones of Bertelli et al. (1994) to relate $T_{\rm eff}$, log g, and [Fe/H] to R. We adopt normal error distributions for $T_{\rm eff}$ and log g, and compute a weighted average of R values that fall within 3 σ of a star's ($T_{\rm eff}$, log g). We only use isochrones within 0.4 dex of a star's [Fe/H] for this calculation. Reddy et al. (2003) describe in more detail the same technique applied to derive stellar ages.

We calculate the final distance by combining the radius, R, with the two estimates of angular diameter, θ. Appendix Data Table 9 lists the distances derived from the Bertelli et al. (1994) isochrones for the non-BHB stars. Distances based on the di Benedetto (1998) S_V-$(V-K)_0$ relationship are on average 20% smaller than those from the Bertelli et al. (1994) isochrones, with an rms scatter of 25%. This internal uncertainty is only a lower limit to the errors in the derived distances, because the two methods share an important error source, the radius estimate. The flux calibration of the spectra introduces additional uncertainty, so these distances should be treated as rough estimates only.

7. BHB CLASSIFICATION

BHB stars comprise only a subset of our blue star sample. Thus, we require a method to estimate surface gravity that is sufficiently accurate to separate the BHB stars from the A dwarfs and blue stragglers also present in our sample.

We use four recent techniques to refine our selection of BHB stars. Kinman et al. (1994) develop the Λ classification, which combines spectrophotometric measures of the size and steepness of the Balmer jump. Wilhelm et al. (1999a) use photometric and spectroscopic measures of $T_{\rm eff}$, log g, and [Fe/H] to select BHB stars. Most recently, Clewley et al. (2002) use a Balmer line-width–color technique and a Balmer line–shape technique that reliably reproduce the Kinman et al. (1994) Λ classification without the need for spectrophotometry. Below, we estimate errors in the application of these techniques to the blue program stars. We compare the results of all four techniques, and make our final selection of BHB stars based on this comparison.

TABLE 3
COMPARISON WITH KINMAN ET AL. 1994

	Brown et al.		Kinman et al.	
ID	BJA_0	$\lambda_{0.5}$	BJA_0	$\lambda_{0.5}$
HD 60778	1.52	27.1	1.37	60.1
HD 64488	1.28	47.9	1.27	64.5
HD 74721	1.44	42.1	1.33	60.2
HD 86986	1.44	39.3	1.33	57.8
HD 105805.....	1.10	51.6	1.07	71.1

NOTE.—Table 3 is presented in its entirety in the electronic edition of the Astronomical Journal. A portion is shown here for guidance regarding its form and content.

7.1. *Kinman et al. Method*

We begin by investigating measures of the size and steepness of the Balmer jump to discriminate BHB stars. Kinman et al. (1994) define a spectrophotometric index, BJA_0, that quantifies the size of the Balmer jump, as well as a parameter, $\lambda_{0.5}$, that measures the slope of the Balmer jump. Both parameters are sensitive to surface gravity. In Table 3 we compare the values of BJA_0 and $\lambda_{0.5}$ that we obtain for 33 BHB/A stars in common with their sample. Our BJA_0 values agree to within a scatter of 5%. However, our values of $\lambda_{0.5}$ are discrepant by 30 ± 40%. The large offset and scatter in $\lambda_{0.5}$ is likely caused by differential atmospheric refraction (we did not observe at the parallactic angle); thus, $\lambda_{0.5}$ is of little use for our application.

The Balmer lines provide another discriminant of BHB stars. A combination of BJA_0 and our spectral type, which is largely driven by the $H_{\rm sum}$ line index for A stars, discriminates well between the 33 Kinman et al. (1994) BHB and A stars that we observed. In our sample there are 41 BHB candidates with $BJA_0 > 1$ mag and spectral type earlier than A2.

7.2. *Wilhelm et al. Method*

Next we investigate using effective temperatures and surface gravities to discriminate BHB stars, following the methods of Wilhelm et al. (1999a).

BHB stars have a well-determined location in the log g-$T_{\rm eff}$ plane. The maximal log g for a ZAHB star is $\log g < (4.33 \log T_{\rm eff} - 13.23)$ (Sweigart 1987). We assign a BHB classification to stars that meet this criterion. Note, however, that the surface gravities of main-sequence stars overlap the surface gravities of BHB stars at large $T_{\rm eff}$. To understand where the log g's overlap, we select "normal" main-sequence A-stars (stars that do not have variability or peculiar metal abundances) from the catalog of Cayrel de Strobel et al. (1997) and find that the minimal log g for main-sequence A stars follows the bounding line $\log g = 4.79 - 1.11 \times 10^{-4}\ T_{\rm eff}$. This relation gives $\log g = 3.7$ for $T_{\rm eff} = 9900$ K. Thus, a star with $\log g > 3.7$ is classified as a main-sequence star unless it overlaps at the hot end with the

BHB trend line, in which case it is labeled BHB/A. We identify 67 BHB candidates with the Wilhelm et al. (1999a) technique.

7.3. *Clewley et al. Methods*

Finally, we investigate using the "$D_{0.15}$-color" and "scale width-shape" methods of Clewley et al. (2002) to discriminate BHB stars from other A-type stars. These methods rely on fitting a Sersic profile to the Hγ and Hδ Balmer lines. The Sersic profile $y = 1-a \exp[(|x-x_0|/b^c]$ depends on three parameters, the line depth, a, the scale length, b, and the power, c, of the profile. We closely follow the procedure described by Clewley et al. (2002) for fitting the Hγ and Hδ profiles, masking metallic blends and iteratively rejecting outliers. Like Clewley et al. (2002), we find that a convolution of a Sersic function and a Gaussian with the FWHM of the Th and Ar lines (2.30 Å) reproduces the observed line shapes very well.

The $D_{0.15}$-color method separates BHB stars based on the width of the Balmer lines (measured at 0.85 of the continuum flux level) and the $(B-V)_0$ color. The line width is sensitive to surface gravity, while the color is (primarily) sensitive to effective temperature. We compute the value of $D_{0.15}$ from the Sersic profile fit, $D_{0.15} = 2b \ln(a/0.15)^{1/c}$, where the line depth $a = 0.83$. We find 56 BHB candidates with the $D_{0.15}$-color method.

The scale width–shape method separates BHB stars based on the scale length b of the Sersic profile, which provides a measure of surface gravity, and the power, c, which provides a measure of effective temperature. BHB stars have $b < 25.7c^3 - 138.2c^2 + 187.5c - 66$ (L. Clewley 2002, private communication), where b is in units of angstroms and c in units of the normalized flux. We find 73 candidates with the scale width–shape method.

According to Clewley et al. (2002), the $D_{0.15}$-color method should select BHB stars with a completeness of ~87% and a contamination rate of ~7% for spectra with S/N = 15. At the same S/N the scale width–shape method should select BHB stars with a completeness of ~82% and a contamination rate of ~12%. This efficiency is similar to the claimed efficiency of BHB selection by Wilhelm et al. (1999a).

7.4. *Final BHB Sample*

All four methods we employ for the identification of BHB stars are sensitive to uncertainties in the parameters derived for the stars. To obtain the purest BHB sample possible, we examine the output samples from each method. Figures 6 and 7 show the results of the four methods for the 33 BHB/

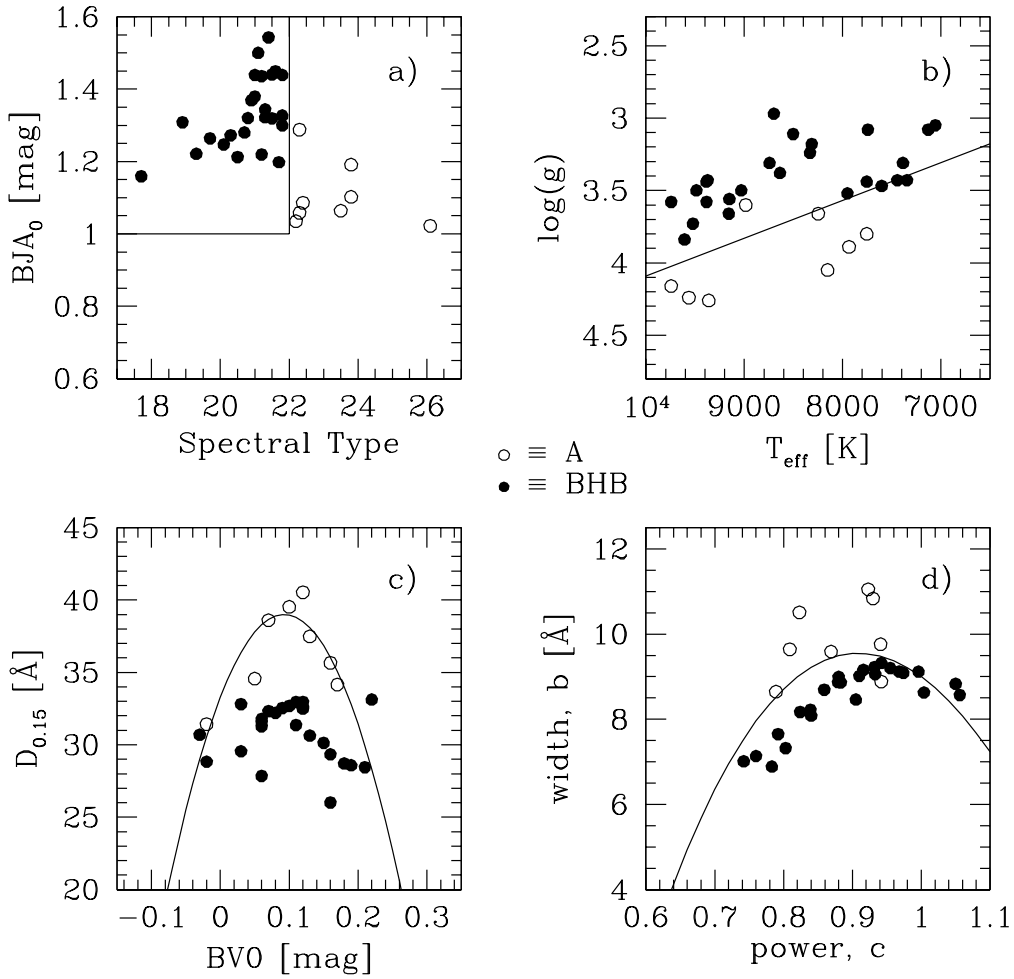

FIG. 6.—Four BHB classification methods applied to the 33 BHB/A stars observed in common with Kinman et al. (1994). (*a*) modified Kinman et al. (1994) method; (*b*) Wilhelm et al. (1999a) method; (*c*) the Clewley et al. (2002) $D_{0.15}$-color method; and (*d*) the Clewley et al. (2002) scale width–shape method. Filled circles mark the BHB stars; open circles mark the A stars.

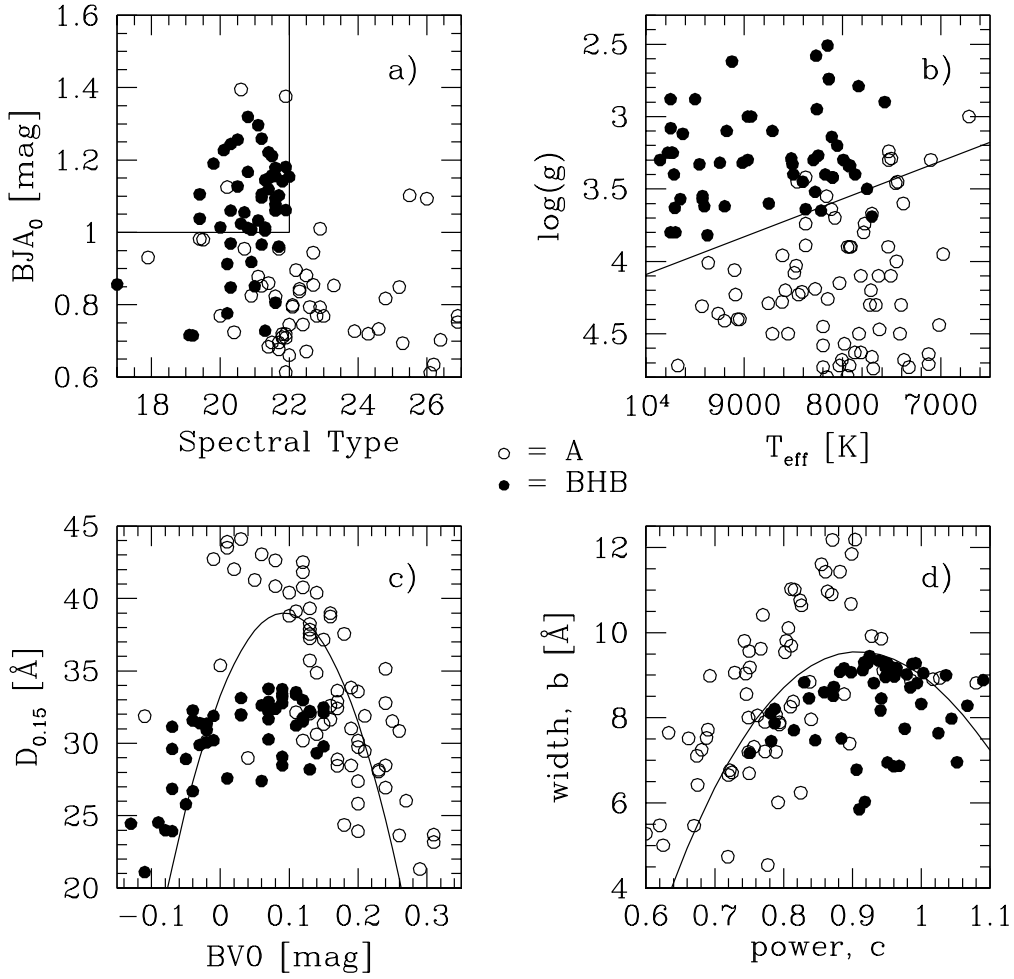

FIG. 7.—Four BHB classification methods applied to the 130 early A-type stars in our sample. The panels are the same as in Fig. 6. Filled circles mark the BHB stars, stars positively classified by three or more of the four methods; open circles mark the other A stars.

A stars in common with Kinman et al. (1994) and for 130 early A-type stars from the Century Survey Galactic Halo Project. The Wilhelm et al. (1999a) method in Figure 7*b* appears to provide the cleanest classification. The Clewley et al. (2002) methods in Figure 7*c* and 7*d* appear to degrade at lower effective temperatures (redder BV0 and lower power *c*).

There are 18 BHB stars in common to all four methods. There are an additional 37 stars selected by three of the four methods. Thus, a total sample of 55 BHB stars is positively classified by three or more of the four methods.

Because all four classification methods start to fail at high temperatures, we can reduce contamination from blue stragglers (at the expense of selecting fewer BHB stars) by imposing a BV0 > 0 mag color limit (see Kinman et al. 1994; Clewley et al. 2002). The BHB sample contains 33 stars in this case. However, the hot BV0 < 0 BHB candidates all have low log g and large BJA$_0$ values. We thus choose not to impose an a priori color limit.

Table 4 summarizes the BHB selection parameters for the 130 early A-type stars in the Century Survey Galactic Halo Project. Column (1) lists the star identification. Column (2)

TABLE 4
THE BHB SELECTION

ID (1)	Type (2)	BJA$_0$ (mag) (3)	(a) (4)	T_{eff} (K) (5)	log g (cm s^{-2}) (6)	(b) (7)	BV0 (mag) (8)	$D_{0.15}$ (Å) (9)	(c) (10)	c (11)	b (Å) (12)	(d) (13)	Total (14)
CHSS 33	21.6 ± 1.2	0.81 ± 0.02	0	9743 ± 200	3.9 ± 0.3	1	−0.02 ± 0.04	31.4 ± 0.5	1	0.96 ± 0.03	9.0 ± 0.2	1	3
CHSS 40	20.3 ± 1.2	1.06 ± 0.02	1	8524 ± 200	3.4 ± 0.3	1	0.13 ± 0.04	32.1 ± 0.5	0	0.86 ± 0.02	8.6 ± 0.1	1	3
CHSS 45	21.2 ± 1.2	1.10 ± 0.02	1	8450 ± 200	3.5 ± 0.3	1	0.11 ± 0.04	33.4 ± 0.5	0	0.92 ± 0.02	9.3 ± 0.1	1	3
CHSS 56	21.8 ± 1.2	1.14 ± 0.02	1	8827 ± 200	3.5 ± 0.3	1	0.08 ± 0.04	32.4 ± 0.5	1	0.95 ± 0.02	9.2 ± 0.2	1	4
CHSS 63	21.2 ± 1.2	1.10 ± 0.02	1	9221 ± 200	3.5 ± 0.3	1	0.09 ± 0.04	29.1 ± 0.4	1	1.09 ± 0.03	8.9 ± 0.1	0	3

NOTE.—Table 4 is presented in its entirety in the electronic edition of the Astronomical Journal. A portion is shown here for guidance regarding its form and content.

TABLE 5

THE BHB STANDARDS

ID (1)	Type (2)	BJA_0 (mag) (3)	(a) (4)	$T_{\rm eff}$ (K) (5)	$\log g$ (cm s^{-2}) (6)	(b) (7)	BV0 (mag) (8)	$D_{0.15}$ (Å) (9)	(c) (10)	c (11)	b (Å) (12)	(d) (13)	Total (14)	Class (15)
HD 60778	21.4 ± 1.2	1.52 ± 0.01	1	7754 ± 200	3.4 ± 0.3	1	0.10 ± 0.04	32.7 ± 0.5	1	0.88 ± 0.01	8.9 ± 0.1	1	4	BHB
HD 64488	22.3 ± 1.2	1.28 ± 0.01	1	8985 ± 200	3.6 ± 0.3	1	−0.02 ± 0.04	31.4 ± 0.4	1	0.94 ± 0.01	8.9 ± 0.1	1	4	$A_{\rm rot}$
HD 74721	21.8 ± 1.2	1.44 ± 0.01	1	8637 ± 200	3.4 ± 0.3	1	0.06 ± 0.04	31.8 ± 0.5	1	0.97 ± 0.02	9.1 ± 0.1	1	4	BHB
HD 86986	21.0 ± 1.2	1.44 ± 0.01	1	7743 ± 200	3.1 ± 0.3	1	0.12 ± 0.04	32.5 ± 0.5	0	0.86 ± 0.01	8.7 ± 0.0	1	3	BHB
HD 105805	23.8 ± 1.2	1.10 ± 0.01	0	7934 ± 200	3.9 ± 0.3	0	0.13 ± 0.04	37.5 ± 0.5	0	0.81 ± 0.00	9.6 ± 0.0	0	0	A
HD 107131	26.1 ± 1.4	1.01 ± 0.01	0	7754 ± 152	3.8 ± 0.3	0	0.17 ± 0.04	34.2 ± 0.5	0	0.79 ± 0.00	8.6 ± 0.0	0	0	A
HD 108382	23.8 ± 1.3	1.19 ± 0.02	0	8247 ± 58	3.7 ± 0.3	1	0.16 ± 0.04	35.7 ± 0.6	0	0.87 ± 0.01	9.6 ± 0.1	0	1	A
HD 109307	23.5 ± 1.2	1.06 ± 0.02	0	8153 ± 200	4.0 ± 0.3	0	0.12 ± 0.04	40.5 ± 0.6	0	0.82 ± 0.00	10.5 ± 0.0	0	0	A
HD 109995	21.5 ± 1.2	1.32 ± 0.01	1	9152 ± 200	3.6 ± 0.3	1	0.08 ± 0.04	32.2 ± 0.5	1	0.93 ± 0.01	9.1 ± 0.1	1	4	BHB
HD 161817	20.7 ± 1.2	1.26 ± 0.01	1	7129 ± 200	3.1 ± 0.3	1	0.16 ± 0.04	29.3 ± 0.5	0	0.84 ± 0.01	8.2 ± 0.1	1	3	BHB
RR7 03	22.2 ± 1.2	1.04 ± 0.03	1	9743 ± 200	4.2 ± 0.3	0	0.05 ± 0.04	34.6 ± 0.6	1	0.94 ± 0.03	9.8 ± 0.3	0	2	A
RR7 15	20.5 ± 1.2	1.21 ± 0.01	1	7386 ± 200	3.3 ± 0.3	1	0.18 ± 0.04	28.7 ± 1.0	0	0.76 ± 0.02	7.1 ± 0.3	1	3	BHB
RR7 23	21.8 ± 1.2	1.30 ± 0.02	1	9157 ± 200	3.7 ± 0.3	1	0.06 ± 0.04	31.3 ± 0.5	1	1.00 ± 0.04	9.1 ± 0.3	0	3	BHB
RR7 36	21.2 ± 1.2	1.22 ± 0.03	1	7602 ± 200	3.5 ± 0.3	1	−0.03 ± 0.04	30.7 ± 0.5	1	0.84 ± 0.02	8.1 ± 0.2	1	4	BHB
RR7 60	19.3 ± 1.2	1.22 ± 0.02	1	7443 ± 200	3.4 ± 0.3	1	0.15 ± 0.04	30.1 ± 0.5	0	0.79 ± 0.02	7.7 ± 0.1	1	3	BHB
RR7 64	21.8 ± 1.2	1.33 ± 0.01	1	7951 ± 1025	3.5 ± 0.3	1	0.22 ± 0.04	33.1 ± 0.5	0	0.88 ± 0.01	9.0 ± 0.1	1	3	BHB
RR7 78	22.4 ± 1.2	1.08 ± 0.01	1	9563 ± 200	4.2 ± 0.3	0	0.07 ± 0.04	38.6 ± 0.5	1	0.93 ± 0.00	10.8 ± 0.0	0	2	A
RR7 91	21.7 ± 1.2	1.20 ± 0.07	1	9608 ± 200	3.8 ± 0.3	1	0.06 ± 0.04	31.6 ± 0.5	1	0.97 ± 0.02	9.1 ± 0.1	1	4	BHB
RR7 103	22.3 ± 1.0	1.06 ± 0.02	1	9361 ± 200	4.3 ± 0.3	0	0.10 ± 0.04	39.5 ± 0.6	0	0.92 ± 0.01	11.0 ± 0.1	0	1	A
SA57 01	20.1 ± 1.2	1.25 ± 0.03	1	7056 ± 200	3.0 ± 0.3	1	0.21 ± 0.04	28.4 ± 1.6	0	0.74 ± 0.04	7.0 ± 0.6	1	3	BHB
SA57 06	21.6 ± 1.2	1.45 ± 0.02	1	8313 ± 200	3.2 ± 0.3	1	0.11 ± 0.04	33.0 ± 0.5	0	0.92 ± 0.01	9.2 ± 0.1	1	3	BHB
SA57 07	21.0 ± 1.2	1.38 ± 0.01	1	9385 ± 200	3.4 ± 0.3	1	−0.02 ± 0.04	28.8 ± 0.5	1	1.05 ± 0.01	8.8 ± 0.1	0	3	BHB?
SA57 17	21.1 ± 1.2	1.50 ± 0.01	1	8503 ± 200	3.1 ± 0.3	1	0.09 ± 0.04	32.5 ± 0.5	1	0.91 ± 0.01	9.0 ± 0.1	1	4	BHB
SA57 49	20.8 ± 1.2	1.32 ± 0.01	1	9487 ± 200	3.5 ± 0.3	1	0.06 ± 0.04	27.8 ± 0.5	1	1.06 ± 0.02	8.6 ± 0.1	0	3	BHB?
SA57 80	21.5 ± 1.2	1.44 ± 0.02	1	8331 ± 200	3.2 ± 0.3	1	0.07 ± 0.04	32.3 ± 0.5	1	0.95 ± 0.02	9.2 ± 0.1	1	4	BHB
M92 I-10	21.3 ± 1.2	1.32 ± 0.02	1	9743 ± 200	3.6 ± 0.3	1	0.03 ± 0.04	29.5 ± 0.4	1	1.00 ± 0.02	8.6 ± 0.1	1	4	BHB
M92 II-23	21.3 ± 1.2	1.34 ± 0.02	1	9384 ± 200	3.6 ± 0.3	1	0.12 ± 0.04	33.0 ± 0.6	0	0.94 ± 0.03	9.3 ± 0.2	1	3	BHB
M92 IV-27	19.7 ± 1.2	1.26 ± 0.03	1	9373 ± 200	3.4 ± 0.3	1	0.11 ± 0.04	31.4 ± 0.5	0	0.82 ± 0.02	8.2 ± 0.1	1	3	BHB
M92 XII-01	17.7 ± 1.2	1.16 ± 0.02	1	7345 ± 200	3.4 ± 0.3	1	0.16 ± 0.04	26.0 ± 1.3	0	0.78 ± 0.04	6.9 ± 0.5	1	3	BHB
M92 XII-09	18.9 ± 1.2	1.31 ± 0.02	1	8699 ± 200	3.0 ± 0.3	1	0.19 ± 0.04	28.6 ± 0.5	0	0.80 ± 0.02	7.3 ± 0.1	1	3	BHB
M92 XII-10	20.3 ± 1.2	1.27 ± 0.03	1	9522 ± 200	3.7 ± 0.3	1	0.13 ± 0.04	30.6 ± 0.5	0	0.91 ± 0.02	8.5 ± 0.1	1	3	BHB
M92 S-20	21.2 ± 1.2	1.44 ± 0.02	1	8743 ± 200	3.3 ± 0.3	1	0.12 ± 0.04	32.6 ± 0.5	0	0.88 ± 0.01	8.9 ± 0.1	1	3	BHB
M92 S-24	20.9 ± 1.2	1.37 ± 0.02	1	9031 ± 200	3.5 ± 0.3	1	0.03 ± 0.04	32.8 ± 0.6	1	0.93 ± 0.03	9.2 ± 0.2	1	4	BHB

lists our spectral type and column (3) lists the BJA_0 value. Column (4) lists a "1" if the star is classified as BHB by the modified Kinman et al. (1994) method (Fig. 7*a*), otherwise it is zero. Column (5) lists the effective temperature and column (6) lists the surface gravity. Column (7) lists a "1" if the star is classified as BHB by the Wilhelm et al. (1999a) method (Fig. 7*b*), otherwise it is zero. Column (8) lists the BV0 color and column (9) lists the $D_{0.15}$ value. Column (10) lists a "1" if the star is classified as BHB by the Clewley et al. (2002) $D_{0.15}$-color method (Fig. 7*c*), otherwise it is zero. Column (11) lists the power c and column (12) lists the scale length b of the Sersic profile fit. Column (13) lists a "1" if the star is classified as BHB by the Clewley et al. (2002) scale width–shape method (Fig. 7*d*), otherwise it is zero. Column (14) is the sum of the four BHB classification methods. We consider the 55 stars selected by three or more of the four methods as BHB stars.

Table 5 summarizes the properties of the 33 BHB/A stars we observed in common with Kinman et al. (1994). The columns are identical with Table 4, with the addition of column (15), which lists the Kinman et al. (1994) classification. All BHB stars are correctly classified as BHB by three or more of the methods, with the exception of HD064488. Kinman et al. (1994) report that HD064488 was formerly classified as a BHB star but is now known to have a high rotation.

8. RESULTS

Figures 8 and 9 show the physical properties of the Century Survey Galactic Halo project stars. Our sample includes thin disk, thick disk, and halo stars.

Figure 8 summarizes the spectral types and the radial velocities (with respect to the local standard of rest) of our sample. Sixty-four percent of the 764 blue stars are F-type stars and 27% are A-type stars. This figure shows a decreasing number of stars from the F types to the A types, until the BHB stars (*filled circles*) appear around spectral type A1.

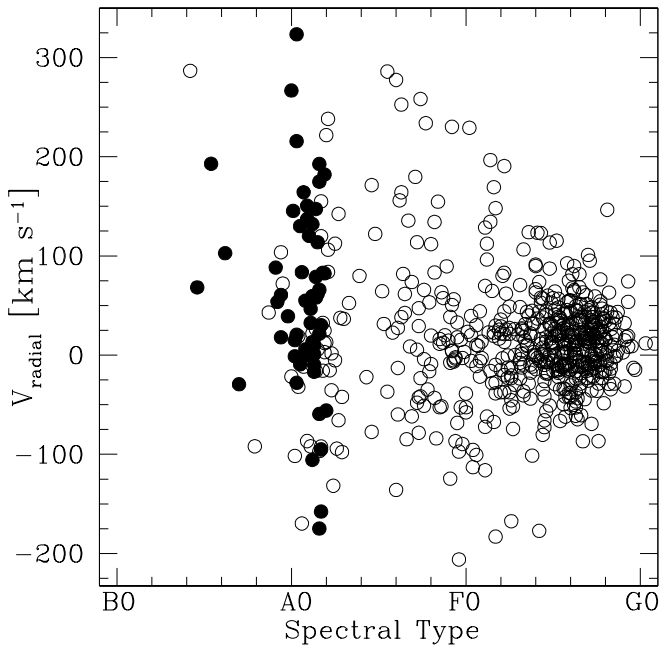

FIG. 8.—Spectral types and radial velocities with respect to the local standard of rest in our sample. Filled circles mark the BHB stars.

Twelve percent of our sample (92 stars) have spectral types between B9 and A3; 55 of these stars are BHB stars. The measured radial velocity dispersion of the BHB stars with respect to the local standard of rest ($\sigma = 97$ km s^{-1}) is consistent with a halo population.

Figure 9 shows the velocities, metallicities, and distances above the Galactic plane, z, for our sample. The clump of stars with $z < 1$ kpc and [Fe/H] > -1 (Fig. 9, *top right*) are the late F types, with a mean BV0 = 0.45 mag, and radial velocity dispersion with respect to the local standard of rest $\sigma = 31$ km s^{-1}. This velocity dispersion is consistent with the $\sim$30 km s^{-1} dispersion measured for $B-V = 0.45$ mag stars in the *Hipparcos* data (Dehnen & Binney 1998), suggesting that the late F types are dwarf stars in the thin and thick disks. The stars with distances extending to $\sim$100 kpc have surface gravities log $g \sim 2.0$ and are likely giants. Our search identifies BHB stars out to a distance of 13 kpc from the Sun. The BHB stars show a wide range of metallicity, $-3 <$ [Fe/H] < 0.

8.1. *Unusual Objects*

One of the benefits of examination of a large sample is the opportunity to identify "unusual" objects. There are 34 objects in our sample that do not have typical A- or F-type spectra. We now examine these objects in detail.

Six of the unusual objects are white dwarfs. McCook & Sion (1999) list five of the white dwarfs as hot DA white dwarfs; one white dwarf appears to be a new discovery. Based on the Wesemael et al. (1993) white dwarf spectral atlas, we classify the object at $13^h10^m13\overset{s}{.}4$, $29°43'59''$ (J2000.0) as a DZ7 white dwarf (Fig. 10).

Four of the unusual objects have normal B-type spectra. Green et al. (1986) identify three objects, for which we measure log $g \sim 2.4$, as horizontal-branch B stars. Our BHB classification also selects these three objects as BHB. The fourth object has a dwarflike log $g = 3.5$, and a spectral classification of B8.5 (Fig. 10). If this star is a main-sequence star, its luminosity places it 0.8 kpc above the Galactic plane. Conlon et al. (1990) publish 32 B stars with similar distances above the Galactic plane, in the range $0.5 < z < 4$ kpc. A late-B star has $\sim$3.5 $M_\odot$ (Cox 2000) and a main-sequence lifetime of $\sim 2 \times 10^8$ yr (Bowers & Deeming 1984). Our B star has a radial velocity +46 km s^{-1}. It has traveled at least 0.8 kpc in 2×10^7 yr, consistent with its inferred lifetime if it formed in the Galactic plane.

Eleven of the unusual objects are hot subdwarfs. Green et al. (1986) classify five subdwarfs as sdB and one as sdO. We follow this classification scheme, and classify the other five objects as sdA, based on their high surface gravities, log $g \sim 5$, and the fact that their Balmer series lines merge into their continua (Fig. 10).

Three of the unusual objects appear to be carbon-enhanced stars. These are identified as stars lying well off the locus of GP versus KP, shown as filled circles in Figure 11. In recent large-scale surveys for metal-poor stars, such carbon-strong stars are found with increasing frequency amongst the lowest metallicity stars (Norris et al. 1997; Rossi et al. 1999). The estimated metallicities of the three carbon-enhanced stars in our sample, are not, however, particularly low, falling in the range $-1.5 <$ [Fe/H]$_F \leq -1.2$.

Of the 10 remaining unusual objects, two appear to be composite spectra with an F-type star plus a star with an

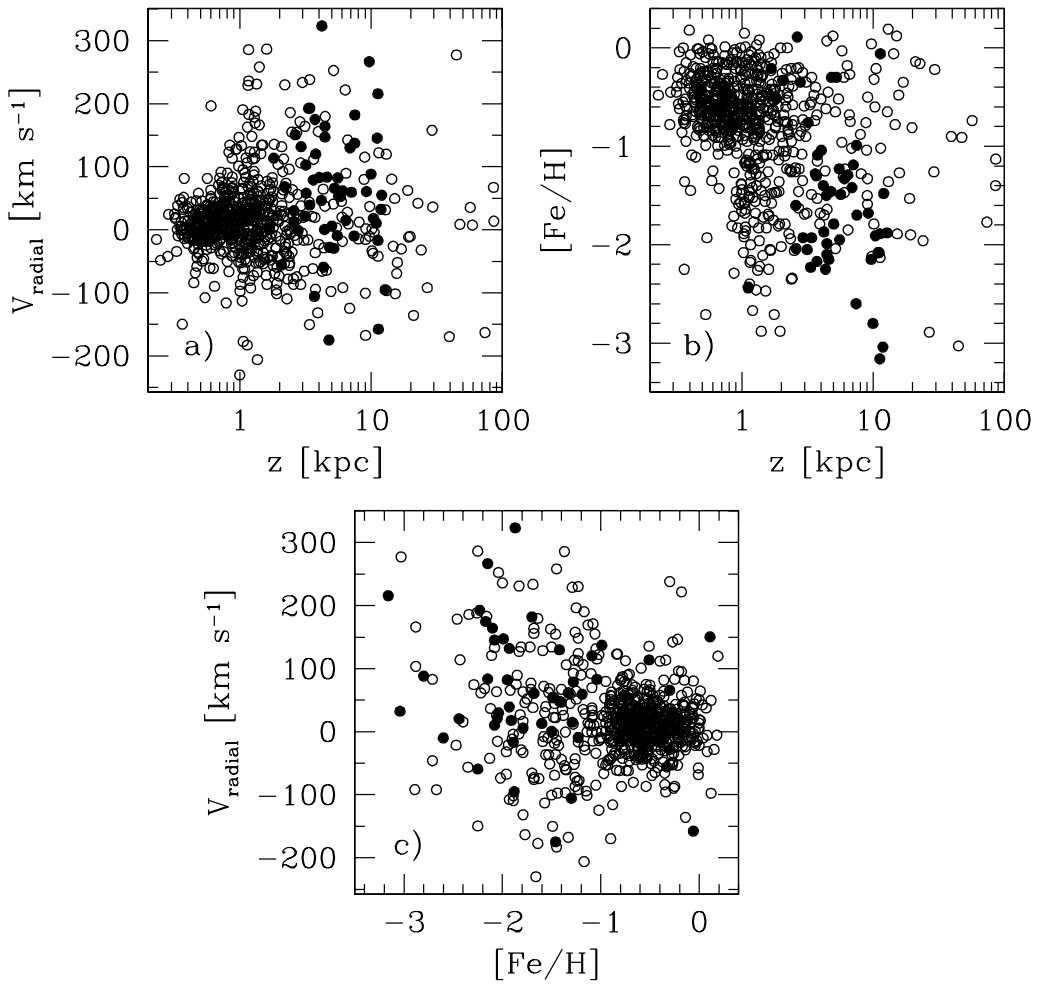

FIG. 9.—Distributions of radial velocity (with respect to the local standard of rest), metallicity, and z distance above the Galactic plane in our sample. Filled circles mark the BHB stars.

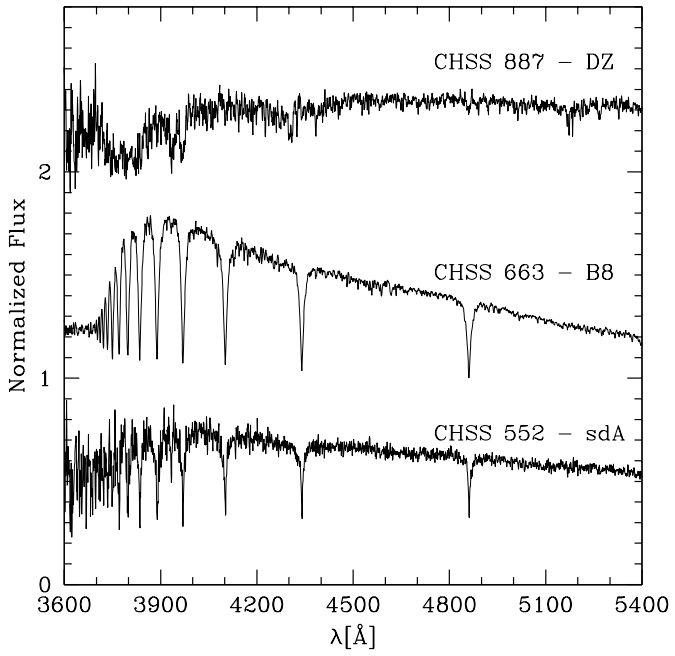

FIG. 10.—Spectra of the DZ7 white dwarf CHSS 887, the B8.5 star CHSS 663, and the sdA object CHSS 552.

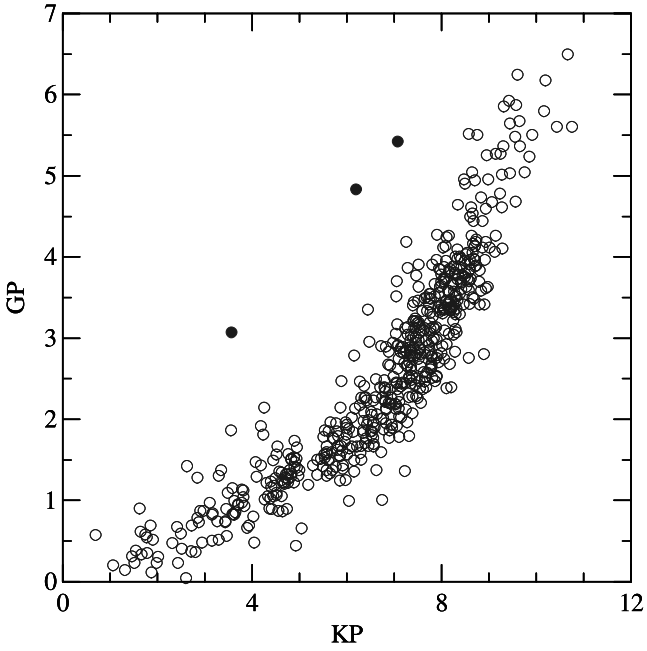

FIG. 11.—GP, the G-band index of Beers et al. (1999), as a function of KP, the Ca II K index. The three carbon-enhanced stars, CHSS 197, CHSS 420, and CHSS 538, are indicated with filled circles.

earlier spectral type. Six of the unusual objects exhibit K-type spectra, but have exceptionally blue colors; the $J-H \simeq -0.9$ Second Data Release 2MASS colors are certainly in error. Two of the unusual objects are extragalactic: one object is a known Seyfert 1 galaxy at $z = 0.33$ (Marziani et al. 1996) and the other is a known quasar at $z = 2.62$ (Barkhouse & Hall 2001).

Table 6 lists the 34 unusual objects. Column (1) is our identifier. Column (2) is our object classification, or the classification found in the literature if available. Column (3) is the J2000.0 right ascension in hours, minutes, and seconds. Column (4) is the J2000.0 declination in degrees, arcminutes, and arcseconds. Column (5) is the V magnitude. Column (6) is the $V-R$ color. Column (7) is the 2MASS Second Data Release J magnitude. Columns (8) and (9) are the 2MASS $J-H$ and $H-K$ colors.

9. CONCLUSIONS

We have observed 764 blue stars as part of the on-going Century Survey Galactic Halo project, a survey of the Milky Way halo and thick-disk populations. The primary part of the sample has $V < 16.5$ mag and $V-R < 0.25$ mag; they are contained within the $1^\circ \times 64^\circ$ Century Survey photometric strip. The secondary part of the sample has $J < 15.0$ mag and $J-H < 0.15$ mag, and lies within the 2MASS region adjacent to the Century Survey. We have discussed our techniques for measuring radial velocities, effective temperatures ($T_{\rm eff}$), surface gravities ($\log g$), metallicities ([Fe/H]), spectral types, and distances from our stellar spectra and colors.

One of our main goals is the identification of a bona fide sample of BHB stars. We thus have devoted special attention to BHB classification. We compare BHB samples selected by the methods of Kinman et al. (1994), Wilhelm et al. (1999a), and Clewley et al. (2002), and identified a combined sample of 55 high-probability BHB stars. The BHB stars comprise 54% of a photometric sample selected on $V-R < 0.10$ mag, $13 < V < 16.5$ mag. Similarly, BHB stars comprise 32% of a photometric sample selected on $J-H < 0.10$ mag, $12 < J < 15$ mag from the 2MASS second data release photometry.

The distances and radial velocities of our sample fit in the standard picture. The late F-type stars are nearby dwarfs in the thin and thick disk. The earlier-type stars, with their wide range of metallicity and velocity, are largely thick-disk and halo stars. The BHB stars range over distances

TABLE 6
Unusual Objects

ID (1)	Object (2)	$\alpha_{\rm J2000.0}$ (3)	$\delta_{\rm J2000.0}$ (4)	V (mag) (5)	$V-R$ (mag) (6)	J (mag) (7)	$J-H$ (mag) (8)	$H-K$ (mag) (9)
CHSS 167	DA3	11 36 14.0	29 01 30	14.87 ± 0.040	−0.15 ± 0.06	14.85 ± 0.04	0.65 ± 0.06	0.12 ± 0.07
CHSS 583	DA2	9 09 19.0	29 29 29	15.80 ± 0.035	−0.14 ± 0.05	...	...	...
CHSS 662	DA6	9 33 41.1	29 11 24	15.96 ± 0.041	0.12 ± 0.07	...	...	...
CHSS 653	DA3	9 32 04.1	28 50 45	16.48 ± 0.034	−0.14 ± 0.05	...	...	...
CHSS 720	DA1	10 02 22.5	29 27 55	16.41 ± 0.031	−0.24 ± 0.05	...	...	...
CHSS 887	DZ7	13 10 13.4	29 43 59	15.91 ± 0.034	0.23 ± 0.05	14.52 ± 0.04	0.32 ± 0.07	−0.05 ± 0.12
CHSS 82	BHB	10 59 28.0	29 25 09	13.54 ± 0.038	−0.13 ± 0.05	13.80 ± 0.03	−0.06 ± 0.05	−0.08 ± 0.07
CHSS 633	B8.5	9 26 15.2	28 03 23	...	...	10.16 ± 0.02	−0.09 ± 0.03	0.00 ± 0.03
CHSS 711	BHB	9 58 15.2	28 52 33	13.04 ± 0.021	−0.07 ± 0.03	13.23 ± 0.03	−0.07 ± 0.05	0.00 ± 0.06
CHSS 748	BHB	10 13 56.3	29 06 15	13.97 ± 0.036	−0.07 ± 0.05	14.17 ± 0.03	−0.15 ± 0.07	0.02 ± 0.09
CHSS 114	sdB	11 13 04.4	29 07 46	14.07 ± 0.032	−0.18 ± 0.05	...	...	...
CHSS 148	sdB	11 28 29.3	29 15 04	15.05 ± 0.027	−0.23 ± 0.04	...	...	...
CHSS 409	sdB	11 08 21.6	29 36 49	15.52 ± 0.029	−0.20 ± 0.04	...	...	...
CHSS 552	sdA	8 57 02.0	29 10 48	15.52 ± 0.024	0.23 ± 0.04	14.60 ± 0.03	0.25 ± 0.05	−0.01 ± 0.07
CHSS 617	sdO	9 23 13.4	29 26 58	14.69 ± 0.033	−0.23 ± 0.05	...	...	...
CHSS 678	sdA	9 38 42.7	29 00 12	14.77 ± 0.030	0.24 ± 0.05	13.89 ± 0.04	0.26 ± 0.06	0.02 ± 0.07
CHSS 773	sdA	10 37 42.0	29 18 22	15.80 ± 0.029	0.22 ± 0.05	14.85 ± 0.04	0.20 ± 0.07	−0.12 ± 0.10
CHSS 800	sdB	11 06 50.5	29 35 32	15.74 ± 0.033	−0.18 ± 0.05	...	...	...
CHSS 808	sdB	11 19 04.8	29 51 53	...	...	14.89 ± 0.04	−0.12 ± 0.09	0.05 ± 0.16
CHSS 846	sdA	12 11 21.0	29 19 28	16.18 ± 0.028	0.17 ± 0.04	...	...	...
CHSS 862	sdA	12 35 17.1	29 02 09	16.12 ± 0.024	0.24 ± 0.04	15.18 ± 0.05	0.07 ± 0.10	0.20 ± 0.13
CHSS 197	Carbon	11 55 09.1	28 58 11	14.90 ± 0.035	0.30 ± 0.05	13.89 ± 0.03	0.23 ± 0.05	0.01 ± 0.06
CHSS 420	Carbon	12 17 38.0	29 18 30	15.53 ± 0.032	0.27 ± 0.05	14.50 ± 0.04	0.30 ± 0.07	0.07 ± 0.09
CHSS 538	Carbon	8 53 24.1	28 44 46	...	...	14.86 ± 0.05	0.15 ± 0.09	0.13 ± 0.12
CHSS 178	Compos.	11 43 37.2	28 56 00	14.45 ± 0.023	0.12 ± 0.04	13.98 ± 0.03	0.15 ± 0.05	0.02 ± 0.06
CHSS 424	Compos.	12 40 27.6	28 54 07	15.66 ± 0.029	0.25 ± 0.05	14.65 ± 0.05	0.12 ± 0.07	0.20 ± 0.09
CHSS 517	K	8 42 25.1	29 13 36	16.22 ± 0.041	−1.01 ± 0.06	...	...	...
CHSS 591	K	9 11 31.7	28 44 40	...	...	12.62 ± 0.02	−0.89 ± 0.14	0.66 ± 0.20
CHSS 615	K	9 22 08.0	27 54 04	...	...	13.68 ± 0.04	−0.95 ± 0.08	0.41 ± 0.16
CHSS 750	K	10 16 46.9	28 11 05	...	...	14.54 ± 0.04	−0.01 ± 0.07	0.77 ± 0.15
CHSS 802	K	11 10 28.1	28 36 08	...	...	14.67 ± 0.04	−0.49 ± 0.09	0.54 ± 0.16
CHSS 807	K	11 18 22.9	30 29 42	...	...	13.30 ± 0.03	−0.84 ± 0.14	0.36 ± 0.22
CHSS 724	Seyfert	10 04 02.6	28 55 35	15.84 ± 0.029	0.25 ± 0.04	...	...	...
CHSS 744	Quasar	10 11 55.6	29 41 42	16.12 ± 0.027	0.16 ± 0.04	...	...	...

Note.—Units of right ascension are hours, minutes, and seconds, and units of declination are degrees, arcminutes, and arcseconds.

$2 < z < 13$ kpc and exhibit a line-of-sight velocity dispersion with respect to the local standard of rest of $\sigma = 97$ km s^{-1}, consistent with a halo population.

In addition, we find 34 unusual objects in our blue-selected sample. One of the unusual objects is a late B star 0.8 kpc above the Galactic plane, and another is a DZ7 white dwarf. We also find three carbon-enhanced, mildly metal-poor stars.

Next, we plan to carry out a kinematic analysis of the Century Survey Galactic Halo Project sample, making use, where available, of recently determined proper motions. We plan to measure the systematic motions of the stars with depth and location along the survey strip. We will look for stars moving together in star streams, and test the possible reality of any detected stream(s).

We are also in the process of extending our observations of the Century Survey Galactic Halo Project. Expanding the survey will allow us to measure structure and systematic motions with higher confidence across a greater arc of the sky.

We thank Perry Berlind and Mike Calkins for obtaining most of the 1.5 m spectra. We thank Stephen Warren and collaborators for making their Sersic profile-fitting routine available to us. We thank John Norris for carrying out the autocorrelation function calculations employed for some of our metallicity determinations. This project makes use of data products from the Two Micron All Sky Survey, which is a joint project of the University of Massachusetts and the Infrared Processing and Analysis Center/California Institute of Technology, funded by NASA and the NSF. This research also makes use of the SIMBAD database, operated at CDS, Strasbourg, France. T. C. B. acknowledges partial support for this work from grants AST 00-98508 and AST 00-98549, awarded by the National Science Foundation. C. A. P. acknowledges partial support for this work from grant AST 00-86321, awarded by the NSF.

APPENDIX

DATA TABLES

Tables 7, 8, and 9 present the photometric and spectroscopic measurements for our blue star sample. The tables contain 737 stars. We exclude 27 unusual objects—the white dwarfs, subdwarfs, K stars, composite spectra, and QSOs—but retain the four B stars and the three carbon-enhanced stars.

Table 7 summarizes the photometry. Column (1) is our identifier. The designation CHSS stands for Century Halo Star Survey and is chosen to be unique from previous surveys. Column (2) is the J2000.0 right ascension in hours, minutes, and seconds. Column (3) is the J2000.0 declination in degrees, arcminutes, and arcseconds. Column (4) is the V magnitude. Column (5) is the $V-R$ color. Column (6) is the BV0 color predicted from Balmer line strengths. Column (7) is the $E(B-V)$ reddening value from Schlegel et al. (1998), reduced according to our distance estimate. Column (8) is the 2MASS Second Data Release J magnitude. Columns (9) and (10) are the 2MASS $J-H$ and $H-K$ colors.

Table 8 summarizes the spectral measurements: the line strengths, the estimated spectral type, and the radial velocity. Column (1) is our identifier. Column (2) is the KP (Ca II) index. Column (3) is the HP2 (Hδ) index. Column (4) is the HG2 (Hγ) index. Column (5) is the GP (G-band) index. Column (6) is the spectral type, where B0 = 10, A0 = 20, F0 = 30, and so forth. Column (7) is the heliocentric radial velocity in kilometers per second.

TABLE 7
PHOTOMETRY

ID (1)	$\alpha_{J2000.0}$ (2)	$\delta_{J2000.0}$ (3)	V (mag) (4)	$V-R$ (mag) (5)	BV0 (mag) (6)	$E(B-V)$ (mag) (7)	J (mag) (8)	$J-H$ (mag) (9)	$H-K$ (mag) (10)
CHSS 1	10 30 13.3	29 20 25	13.74 ± 0.027	0.29 ± 0.04	0.50	0.02	12.71 ± 0.03	0.30 ± 0.04	0.05 ± 0.04
CHSS 2	10 31 03.4	29 24 39	13.17 ± 0.027	0.28 ± 0.04	0.48	0.02	12.10 ± 0.02	0.31 ± 0.03	0.04 ± 0.03
CHSS 3	10 31 11.6	29 16 23	14.67 ± 0.027	0.27 ± 0.04	0.47	0.02	13.66 ± 0.03	0.27 ± 0.04	0.06 ± 0.04
CHSS 4	10 31 19.9	29 22 23	14.85 ± 0.027	0.28 ± 0.04	0.47	0.02	13.87 ± 0.03	0.29 ± 0.04	0.04 ± 0.05
CHSS 5	10 31 23.5	29 35 17	13.72 ± 0.037	0.30 ± 0.06	0.47	0.02	12.71 ± 0.03	0.25 ± 0.04	0.06 ± 0.04

NOTE.—Table 7 is presented in its entirety in the electronic edition of the Astronomical Journal. A portion is shown here for guidance regarding its form and content.

TABLE 8
SPECTROSCOPIC MEASUREMENTS

ID (1)	KP (2)	HP2 (3)	HG2 (4)	GP (5)	Type (6)	V_{radial} (km s^{-1}) (7)
CHSS 1	8.14	3.03	3.18	3.58	36.4 ± 1.5	43.9 ± 9.7
CHSS 2	7.96	3.42	3.39	3.32	36.6 ± 1.6	−18.9 ± 9.5
CHSS 3	7.81	3.37	3.84	2.51	35.8 ± 1.5	13.9 ± 10.3
CHSS 4	7.05	3.35	3.43	3.51	35.7 ± 1.4	−62.7 ± 10.6
CHSS 5	8.42	3.31	3.21	3.68	37.3 ± 1.5	42.3 ± 9.5

NOTE.—Table 8 is presented in its entirety in the electronic edition of the Astronomical Journal. A portion is shown here for guidance regarding its form and content.

TABLE 9
STELLAR PARAMETERS

ID (1)	$T_{\rm eff}$ (K) (2)	log g cm s^{-2} (3)	[Fe/H]$_{\rm GA}$ (4)	[Fe/H]$_{\rm KP}$ (5)	[Fe/H]$_{\rm EC}$ (6)	[Fe/H]$_{\rm final}$ (7)	Dist. (kpc) (8)	M_V (mag) (9)
CHSS 1[a].....	6013	4.25	−0.51	−0.87	−0.77	−0.69	0.72	4.37
CHSS 2[a].....	6088	4.56	−0.39	−0.78	−0.87	−0.59	0.67	3.97
CHSS 3[a].....	6182	4.48	−0.44	−0.57	−0.84	−0.51	1.26	4.10
CHSS 4[a].....	6095	4.45	−0.82	−0.80	−0.75	−0.81	1.26	4.29
CHSS 5[a].....	6148	4.70	−0.45	−0.34	−0.19	−0.40	0.86	3.97

NOTE.—Table 9 is presented in its entirety in the electronic edition of the Astronomical Journal. A portion is shown here for guidance regarding its form and content.

[a] Spectrum observed in nonphotometric conditions.

Table 9 summarizes the stellar parameters. Column (1) is our identifier. Column (2) is the effective temperature in kelvins. Column (3) is the surface gravity in centimeter per second. Columns (4) through (6) are the metallicities derived based on the genetic algorithm (GA), the KP index (KP), and the equivalent widths/χ^2 spectral match procedure (EC). Metallicities are given as the logarithmic [Fe/H] ratio relative to the Sun. Column (7) is the average [Fe/H] we take as the final value, as described in § 4. Column (8) is the estimated distance in kiloparsecs, as described in § 6. Objects with spectra obtained in nonphotometric conditions are marked and have increased uncertainty in their distance estimates. Column (9) is the absolute M_V magnitude corrected for reddening, given the estimated distance. When we do not have V photometry, we use the 2MASS J magnitude and add the mean $V-J$ color for the measured spectral type to estimate M_V.

REFERENCES

Allende Prieto, C. 2003, MNRAS, 339, 1111
Allende Prieto, C., & Lambert, D. L. 1999, A&A, 352, 555
Alonso, A., Arribas, S., & Martínez-Roger, C. 1996, A&A, 313, 873
Alonso, A., ———. 1999, A&AS, 140, 261
Arnold, R., & Gilmore, G. 1992, MNRAS, 257, 225
Barkhouse, W. A., & Hall, P. B. 2001, AJ, 121, 2843
Barklem, P. S., Piskunov, N., & O'Mara, B. J. 2000, A&AS, 142, 467
Barklem, P. S., Stempels, H. C., Allende Prieto, C., Kochukhov, O. P., Piskunov, N., & O'Mara, B. J. 2002, A&A, 385, 951
Beers, T. C., Drilling, J. S., Rossi, S., Chiba, M., Rhee, J., Führmeister, B., Norris, J. E., & von Hippel, T. 2002, AJ, 124, 931
Beers, T. C., Kage, J. A., Preston, G. W., & Shectman, S. A. 1990, AJ, 100, 849
Beers, T. C., Rossi, S., Norris, J. E., Ryan, S. G., & Shefler, T. 1999, AJ, 117, 981
Bertelli, G., Bressan, A., Chiosi, C., Fagotto, F., & Nasi, E. 1994, A&AS, 106, 275
Bowers, R. L. & Deeming, T. 1984, Astrophysics: Stars, Volume 1 (Boston: Jones and Bartlett)
Brown, P. J. F., Dufton, P. L., Keenan, F. P., Boksenberg, A., King, D. L., & Pettini, M. 1989, ApJ, 339, 397
Brown, W. R., Geller, M. J., Fabricant, D. G., & Kurtz, M. J. 2001, AJ, 122, 714
Caloi, V., D'Antona, F., & Mazzitelli, I. 1997, A&A, 320, 823
Carney, B. W., Storm, J., & Jones, R. V. 1992, ApJ, 386, 663
Carney, B. W., Wright, J. S., Sneden, C., Laird, J. B., Aguilar, L. A., & Latham, D. W. 1997, AJ, 114, 363
Carroll, T. A., & Staude, J. 2001, A&A, 378, 316
Cassisi, S., Castellani, V., degl'Innocenti, S., Salaris, M., & Weiss, A. 1999, A&AS, 134, 103
Cayrel de Strobel, G., Soubiran, C., Friel, E. D., Ralite, N., & Francois, P. 1997, A&AS, 124, 299
Clementini, G., Gratton, R., Bragaglia, A., Carretta, E., Di Fabrizio, L., & Maio, M. 2003, AJ, 125, 1309
Clewley, L., Warren, S. J., Hewett, P. C., Norris, J. E., Peterson, R. C., & Evans, N. W. 2002, MNRAS, 337, 87
Conlon, E. S., Dufton, P. L., Keenan, F. P., & Leonard, P. J. T. 1990, A&A, 236, 357
Cox, A. N. 2000, Allen's Astrophysical Quantities (4th ed.; New York: Springer)
Dehnen, W. & Binney, J. J. 1998, MNRAS, 298, 387
di Benedetto, G. P. 1998, A&A, 339, 858
Fabricant, D., Cheimets, P., Caldwell, N., & Geary, J. 1998, PASP, 110, 79
Fekel, F. C. 1999, in IAU Colloq. 170, Precise Stellar Radial Velocities, ed. J. B. Hearnshaw & C. D. Scarfe (ASP Conf. Ser. 185) (San Francisco: ASP), 378
Geller, M. J., et al. 1997, AJ, 114, 2205
Gilmore, G., Wyse, R. F. G., & Norris, J. E. 2002, ApJ, 574, L39
Gould, A., & Popowski, P. 1998, ApJ, 508, 844
Gray, R. O., & Corbally, C. J. 1994, AJ, 107, 742
Green, R. F., Schmidt, M., & Liebert, J. 1986, ApJS, 61, 305
Hubeny, I., & Lanz, T. 2000, SYNSPEC: A User's Guide
Ibata, R. A., Gilmore, G., & Irwin, M. J. 1994, Nature, 370, 194
Ibata, R., Irwin, M., Lewis, G. F., & Stolte, A. 2001, ApJ, 547, L133
Ivezić, Ž., et al. 2000, AJ, 120, 963
Jacoby, G. H., Hunter, D. A., & Christian, C. A. 1984, ApJS, 56, 257
Johnston, K. V., Hernquist, L., & Bolte, M. 1996, ApJ, 465, 278
King, J. R. 1997, AJ, 113, 2302
Kinman, T. D., Pier, J. R., Suntzeff, N. B., Harmer, D. L., Valdes, F., Hanson, R. B., Klemola, A. R., & Kraft, R. P. 1996, AJ, 111, 1164
Kinman, T. D., Suntzeff, N. B., & Kraft, R. P. 1994, AJ, 108, 1722
Kurtz, M. J., & Mink, D. J. 1998, PASP, 110, 934
Kurucz, R. L. 1993, CD-ROM 18, SYNTHE Spectrum Synthesis Programs and Line Data (Cambridge: Smithsonian Astrophys. Obs.)
Lance, C. M. 1988, ApJS, 68, 463
Lindegren, L., & Dravins, D. 2003, A&A, 401, 1185
Majewski, S. R. 1993, ARA&A, 31, 575
Majewski, S. R., Munn, J. A., & Hawley, S. L. 1996, ApJ, 459, L73
Marziani, P., Sulentic, J. W., Dultzin-Hacyan, D., Calvani, M., & Moles, M. 1996, ApJS, 104, 37
Massey, P., Strobel, K., Barnes, J. V., & Anderson, E. 1988, ApJ, 328, 315
McCook, G. P., & Sion, E. M. 1999, ApJS, 121, 1
Muller, G. P., Reed, R., Armandroff, T., Boroson, T. A., & Jacoby, G. H. 1998, in Proc. SPIE, 3355, 577
Newberg, H. J., et al. 2002, ApJ, 569, 245
Norris, J. E., & Hawkins, M. R. S. 1991, ApJ, 380, 104
Norris, J. E., Ryan, S. G., & Beers, T. C. 1997, ApJ, 488, 350
O'Connell, W. O. R. 1973, AJ, 78, 1074
Pier, J. R. 1982, AJ, 87, 1515
Preston, G. W., Beers, T. C., & Shectman, S. A. 1994, AJ, 108, 538
Preston, G. W., Shectman, S. A., & Beers, T. C. 1991, ApJ, 375, 121
Preston, G. W., & Sneden, C. 2000, AJ, 120, 1014
Reddy, B. E., Tomkin, J., Lambert, D. L., & Allende Prieto, C. 2003, MNRAS, 340, 304
Rodgers, A. W. 1971, ApJ, 165, 581
Rodgers, A. W., Roberts, W. H., & Walker, I. 1993, AJ, 106, 591
Rossi, S., Beers, T. C., & Sneden, C. 1999, in ASP Conf. Ser. 165, The Third Stromlo Symposium: The Galactic Halo, ed. B. K. Gibson, T. S. Axelrod, & M. E. Putnam (San Francisco: ASP), 264
Salaris, M., degl'Innocenti, S., & Weiss, A. 1997, ApJ, 479, 665
Sandage, A. 1993, AJ, 106, 703
Schlegel, D. J., Finkbeiner, D. P., & Davis, M. 1998, ApJ, 500, 525
Searle, L., & Zinn, R. 1978, ApJ, 225, 357
Skrutskie, M. F., et al. 2000, VizieR Online Data Catalog
Sommer-Larsen, J., Christensen, P. R., & Carter, D. 1989, MNRAS, 238, 225

Stefanik, R. P., Latham, D. W., & Torres, G. 1999, in IAU Colloq. 170, Precise Stellar Radial Velocities, ed. J. B. Hearnshaw & C. D. Scarfe (ASP Conf. Ser. 185) (San Francisco: ASP), 354
Sweigart, A. V. 1987, ApJS, 65, 95
Udry, S., Mayor, M., & Queloz, D. 1999, in IAU Colloq. 170, Precise Stellar Radial Velocities, ed. J. B. Hearnshaw & C. D. Scarfe (ASP Conf. Ser. 185) (San Francisco: ASP), 367
Vivas, A. K., et al. 2001, ApJ, 554, L33
Vivas, A. K., & Zinn, R. 2003, preprint (astro-ph/0212116)
Wesemael, F., Greenstein, J. L., Liebert, J., Lamontagne, R., Fontaine, G., Bergeron, P., & Glaspey, J. W. 1993, PASP, 105, 761
Wilhelm, R., Beers, T. C., & Gray, R. O. 1999a, AJ, 117, 2308
Wilhelm, R., Beers, T. C., Sommer-Larsen, J., Pier, J. R., Layden, A. C., Flynn, C., Rossi, S., & Christensen, P. R. 1999b, AJ, 117, 2329
Wilson, R. E. 1963, General Catalogue of Stellar Radial Velocities (Washington: Carnegie Inst. Washington)
Worthey, G., Faber, S. M., Gonzalez, J. J., & Burstein, D. 1994, ApJS, 94, 687
Yanny, B., et al. 2000, ApJ, 540, 825
———. 2003, ApJ, 588, 824